DALHOUSIE UNIVERSITY

Geological controls on radon concentration in surficial sediment in Whitehorse, Yukon

Michael J. Kishchuk

SUBMITTED IN PARTIAL FULFILLMENT OF THE REQUIREMENTS FOR
THE DEGREE OF BACHELOR OF SCIENCE, HONOURS
DEPARTMENT OF EARTH AND ENVIRONMENTAL SCIENCES
DALHOUSIE UNIVERSITY, HALIFAX, NOVA SCOTIA

April 2021

DALHOUSIE UNIVERSITY

Department of Earth and Environmental Sciences
Halifax, Nova Scotia, Canada
B3H 4R2
(902) 494-2358

DATE: 23 April 2021

AUTHOR: Michael Kishchuk

TITLE: Geological controls on radon concentration in surficial sediment in Whitehorse, Yukon

Degree: B. Sc. Honours Earth Sciences Convocation: May Year: 2021

Distribution License

DalSpace requires agreement to this non-exclusive distribution license before your item can appear on DalSpace.

NON-EXCLUSIVE DISTRIBUTION LICENSE

You (the author(s) or copyright owner) grant to Dalhousie University the non-exclusive right to reproduce and distribute your submission worldwide in any medium.

You agree that Dalhousie University may, without changing the content, reformat the submission for the purpose of preservation.

You also agree that Dalhousie University may keep more than one copy of this submission for purposes of security, back-up and preservation.

You agree that the submission is your original work, and that you have the right to grant the rights contained in this license. You also agree that your submission does not, to the best of your knowledge, infringe upon anyone's copyright.

If the submission contains material for which you do not hold copyright, you agree that you have obtained the unrestricted permission of the copyright owner to grant Dalhousie University the rights required by this license, and that such third-party owned material is clearly identified and acknowledged within the text or content of the submission.

If the submission is based upon work that has been sponsored or supported by an agency or organization other than Dalhousie University, you assert that you have fulfilled any right of review or other obligations required by such contract or agreement.

Dalhousie University will clearly identify your name(s) as the author(s) or owner(s) of the submission, and will not make any alteration to the content of the files that you have submitted.

If you have questions regarding this license please contact the repository manager at dalspace@dal.ca.

Grant the distribution license by signing and dating below.

_____ _____

Name of signatory Date

Abstract

Indoor concentrations of radon gas in excess of Health Canada guidelines have been reported throughout the Whitehorse area, yet only cursory measurements have been made to determine the concentration of radon in undisturbed near-surface settings. Radon-222 is a carcinogenic gas produced by the decay of ^{226}Ra as part of the ^{238}U decay series. Exposure to radon and its radioactive daughters is the second-leading cause of lung cancer in Canada. Information about its occurrence is therefore important for public health and for policies such as building codes. Low concentrations of uranium in bedrock underlying the Whitehorse region suggest that surficial sediment may be a primary local source of ^{222}Rn.

To evaluate radon sources and activity, 30 sites representing a range of bedrock and surficial sediment types were evaluated in the summer of 2020. The underlying bedrock lithologies are granodiorite, limestone, clastic sediments, and basalt. The surficial sediment types include lodgement till, glaciofluvial sand and gravel, glaciolacustrine fine sand and silt, fluvial sand and gravel, and eolian sand. To determine controlling factors, mean radon concentration at each site was compared to bedrock lithology, surficial sediment composition, type, and thickness, grain size distribution, sediment maturity, soil moisture, matrix geochemistry, and clast geochemistry.

A positive correlation was observed between grain size distribution and radon concentration, with sediments containing more silt and clay in their matrix displaying higher radon concentration, and this may be due to the decreased permeability of clay-rich sediments. Radon concentration is generally higher in less mature sediments (e.g. till) compared to more mature sediments (e.g. fluvial and eolian sand), suggesting that less weathered sediment types may produce more radon. No significant correlation was observed between radon concentration and bedrock lithology nor depth to bedrock, possibly because sediment thickness in the Whitehorse region exceeds the distance radon can travel before it decays. Pronounced interseasonal variation was observed at three long-term monitoring sites, with little intraseasonal variation over the summer. This variation may be caused by seasonal freezing and thawing of the ground, an important consideration in northern landscapes. Geochemical analysis suggests that while some radon may be produced in near-surface settings, the controls examined in this study are primarily controls on transport. Sediment maturity and grain size are first order controlling factors of radon concentration in surficial sediment and bedrock is neither the only nor the most important source of radon in the study area.

Keywords:
radon, glaciated landscapes, grain size distribution, sediment maturity, seasonal variation

Table of Contents

List of Figures

List of Tables

Acknowledgements

I was mentored, supported, and carried by the generosity and expertise of many people this year. John Gosse was an excellent guide and supervisor, even from a distance, even in these strangest of semesters. I learned so much from him. Many thanks to Panya Lipovsky and Jeff Bond for providing me with a project in a pandemic year, and for supporting me through the summer. Additional thanks to Panya for producing Figures 1, 2, and 3. Thanks to Derek Cronmiller for reviewing an earlier version of this manuscript, to Karen MacFarlane for copy-editing it, and to other staff at the YGS for their interest and insight in my project this summer. Brad Harvey at GSC Ottawa kindly loaned the sampling equipment and resupplied us with probes partway through the summer. It has been challenging to write and learn away from campus this year, and the CRISDal Lab group provided much-appreciated feedback and support all the way through. Thank you all.

Field work took place on the traditional territories of the Kwanlin Dün and Ta'an Kwäch'än First Nations, and this thesis was written in K'jipuktuk, on unceded Mi'kmaq territory.

Endless thanks to Paul Kishchuk and Kristina Craig of Whitehorse, for loaning me their truck, for providing lodging and food free of charge, for their love and support, etc.
Funding for analyses was provided by YGS, and funding to Michael Kishchuk was provided jointly by YGS and NSERC.

1. Introduction

Radon is a colourless, odourless carcinogenic gas which occurs naturally in soil and rock. While not dangerous in outdoor settings (where it dissipates quickly), radon poses a major public health hazard when it accumulates in buildings. Typically it enters via openings and cracks in foundations, and can become trapped in poorly ventilated basements. It is the leading cause of lung cancer among non-smokers, causing over 3 000 deaths annually in Canada (Government of Canada, 2020). The alpha decay of inhaled radon damages lung tissue, and after inhalation this pulmonary harm is compounded by its daughters ^{210}Po, ^{214}Pb, ^{214}Bi and ^{214}Po. These adhere to aerosols and accumulate in the lungs where they in turn produce alpha, beta, and gamma radiation (Porstendorfer, 1994). As of 2018, nearly 4 400 Yukon homes have been tested for indoor radon, with more than 3 300 measurements in the greater Whitehorse area (Yukon Housing Corporation, 2018). Of these, 17 of 44 subdivisions (Fig. 1) have average indoor radon concentrations in excess of Health Canada's guideline of 200 Bq m^{-3} (Government of Canada, 2020). It is worth noting that the World Health Organization (WHO) hazard threshold is even lower than the Canadian guideline, recommending mitigation if indoor radon concentration exceeds 100 Bq m^{-3} (World Health Organization, 2009).

While many international studies assume that bedrock uranium concentration is the strongest control on radon concentration in urban regions (e.g., Stanley *et al*., 2019; Cinelli *et al.*, 2015), several authors have argued that attention must also be given to the overlying surficial sediment (e.g. Thu *et al*., 2020; Nazaroff 1992). This is particularly important in areas where sediment cover is thicker than the diffusion distance of radon over its radioactive lifetime (the half-life ($t_{½}$) and mean lifetime of ^{222}Rn are 3.8 days and 5.5 days respectively (Marin, 1956)). In these areas, the physical and chemical properties of the surficial cover could potentially control radon flux. Additionally, uranium concentration in the Whitehorse suite of granitoid rocks is generally low (Yukon Geological Survey, 2020b), suggesting non-bedrock radon sources. A comparison of variation in radon gas concentration with properties of the surficial cover is therefore warranted for the Whitehorse region.

The effects of sediment grain size and water content on radon emanation are well-established (e.g. Thu *et al*., 2020; Sakoda *et al*., 2010; Markannen and Arvela, 1992). Such studies are typically based on numerical modelling and laboratory experiments, and there is a

paucity of field data relating to these factors, especially in the variable sediment types of glaciated landscapes. I therefore undertook a field sampling program which measured soil radon in situ, while also collecting a wide range of environmental data. I hypothesize that the grain size distribution of surficial sediments is the strongest control on near-surface radon concentration.

Knowledge of radon source and distribution is necessary for public health policy involving building codes and workplace conditions. The results of this thesis also contribute to a current Yukon Geological Survey program aiming to better understand the distribution of radon in surficial materials in the territory. This compares the effect of several geological and meteorological controls on spatial and temporal variability in the flux of soil radon gas in the Whitehorse study area (Fig. 1), with a long-term goal of understanding how to better predict and mitigate regional risks associated with radon. By measuring radon in different representative undisturbed surficial sediment types, and by documenting which factors have first-order control on soil radon flux variability, it may be possible predict where and when radon is likely to exceed concentration guidelines, and perhaps extrapolate radon concentration in untested regions of the territory. My preliminary results reveal that radon flux varies seasonally in some (but not all) surficial sediments, and that spatial variation is at least partly related to sediment grain-size distribution and maturity. Since the composition and thickness of surficial deposits throughout Yukon are non-uniform, these initial findings may provide direction for future Yukon Geological Survey research and perhaps for other national and international studies in regions with similar sediment types and thickness.

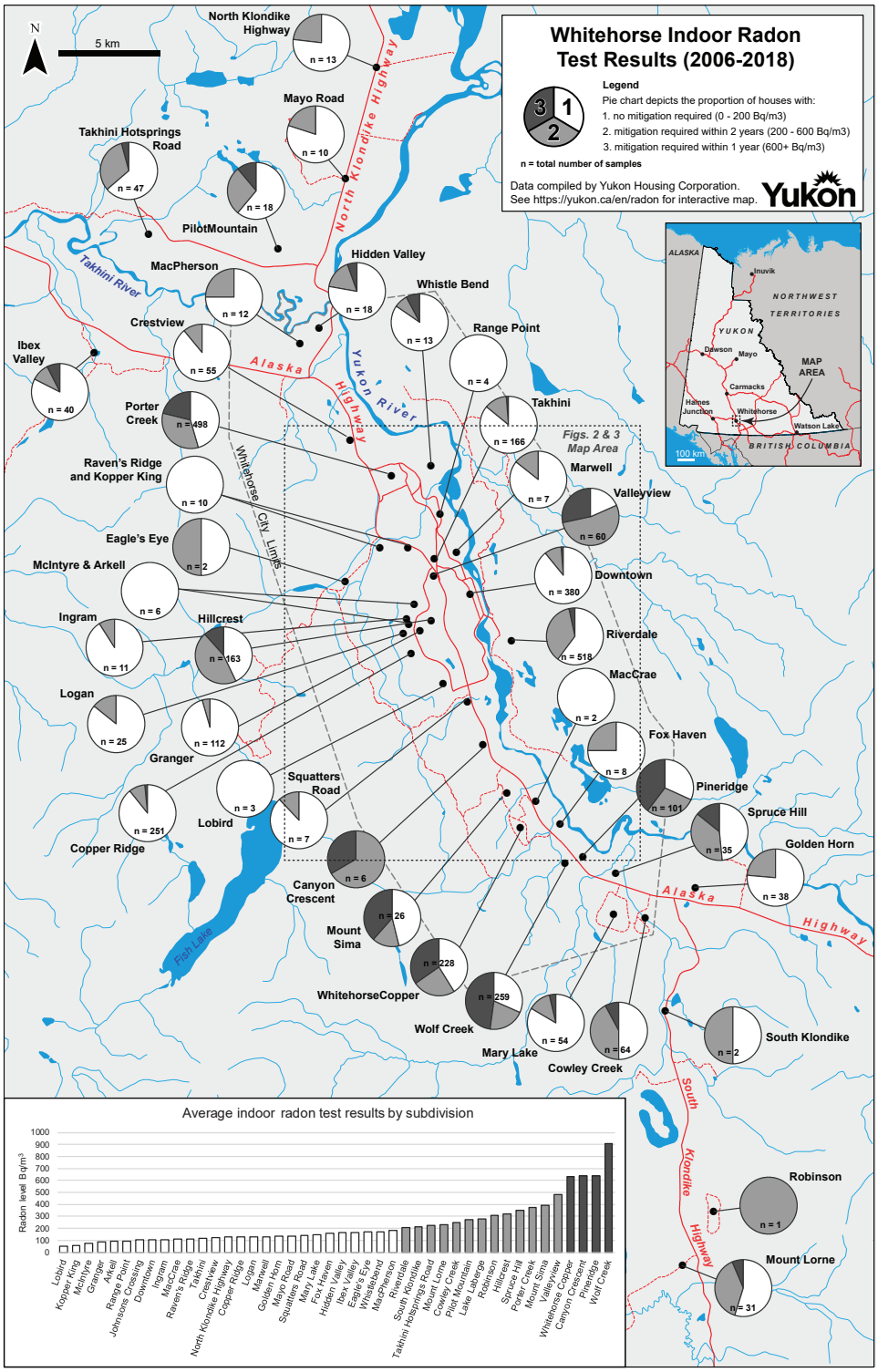

Figure 1 – Distribution and results of indoor radon tests compiled by Yukon Housing Corporation for the period 2006-2018 (Yukon Housing Corp., 2018a). Sites in this study are located in Whistle Bend, Porter Creek, Raven's Ridge, Takhini, Granger, Copper Ridge, Riverdale, Squatters Road, Mount Sima, and Wolf Creek.

2. Background

2.1 Geologic setting

2.1.1 Bedrock geology

Four bedrock lithologic units underlie the Whitehorse area (Hart and Radloff, 1990; Colpron, 2011; Yukon Geological Survey, 2020a): the Hancock member limestone and the Mandanna member clastic sediments of the Aksala Formation, the Whitehorse batholith granitoids, and the Miles Canyon Basalt (Fig. 2). The Hancock and Mandanna members of the Aksala Formation were deposited during the upper Triassic in a coastal fluvial setting. The Hancock member is composed of massive and thickly bedded limestone with some dolostone, limestone debris flow conglomerate, and minor chert. The Mandanna member is composed of sandstone and polymictic conglomerate, along with mudstone and minor bioturbated sandstone. The Whitehorse batholith intruded these Triassic units in the mid-Cretaceous, between 112 and 105 Ma, and in the study area these rocks are characterized as medium to coarse-grained granodiorite and diorite (Colpron 2011). During the Miocene and Pliocene, the Miles Canyon Basalt flowed northward from a vent near Mount Sima and has thicknesses of up to 110 m (Pearson *et al.*, 2001).

2.1.2 Surficial geology

The surficial geology of the Whitehorse area records a complex history of deposition by ice, water, and wind (Fig. 3). The McConnell Glaciation, which occurred from roughly 23.9 to 10.7 ka, was the most recent glaciation of the Whitehorse area (Bond, 2004). Ice flowed northward from the Coast Mountain and Cassiar lobes of the Cordilleran Ice Sheet and reached a glacial maximum by at least 18 ka. At this time, the Whitehorse valley was completely covered by ice. During deglaciation the ice underwent a fluctuating recession characterized by periods of stagnation and readvance. During periods of stagnation, several large glacial lakes formed in the Whitehorse area (Bond, 2004).

A range of sediment types were sampled at the 30 sites in this study, including diamicton, bedded and massive sands, fine-grained sands and silts, and moderately sorted gravel units. The genesis of the sediments have been previously interpreted by Bond *et al.*, (2005a–c) as till,

glaciofluvial sand and gravel, fine-grained glaciolacustrine sediment (sand, silt and clay), post-glacial fluvial sand and gravel, and eolian sand.

Diamictons away from slopes in the Whitehorse area are typically dense, unsorted, and matrix-supported with a sandy silt matrix and most clasts derived from glacially-eroded bedrock, and are thus considered lodgement tills. In this thesis, I have distinguished diamicton colluvium deposited at the base of slopes from the more compact original tills since resedimentation has undoubtedly altered their compaction, and since sorting processes may have altered their chemical composition compared to non-colluviated tills.

Glaciofluvial gravels were deposited in terraces, kettled ice-contact complexes, and outwash channels as the ice receded, and are typically composed of moderately sorted rounded pebbles and cobbles with a sandy matrix. A thick package of glaciolacustrine sand, silt and clay was deposited at the bottom of Glacial Lake Laberge, covering much of the Whitehorse valley. Dammed by ice to the south and a recessional moraine at the north end of Lake Laberge, this glacial lake occupied the Whitehorse valley bottom during deglaciation (Brideau *et al.*, 2011). Shoreline deposits tend to be coarser and the lake sediments fine upward, reflecting the recession of the ice sheet and associated melt-water input to the Lake. As Glacial Lake Laberge drained, the Yukon River delta prograded northward with the lowering shoreline, depositing a veneer of fluvial sand on top of the lacustrine sediment. Winds reworked exposed riverbed sand and re-deposited it subaerially as dunes (Wolfe *et al.*, 2011).

A veneer of fine-grained sandy silt loess derived from deflation of the paraglacial surface was also deposited over much of the study area. These deposits range from 10 to 50 cm thick. The Yukon River has since incised the thick glaciolacustrine deposits during the Holocene, forming sand and gravel cut-and-fill terraces inset into the last glacial maximum terrace and adjacent to the modern floodplain. The thickness of these deposits vary with the topography of the underlying bedrock and can exceed thicknesses of 100 m.

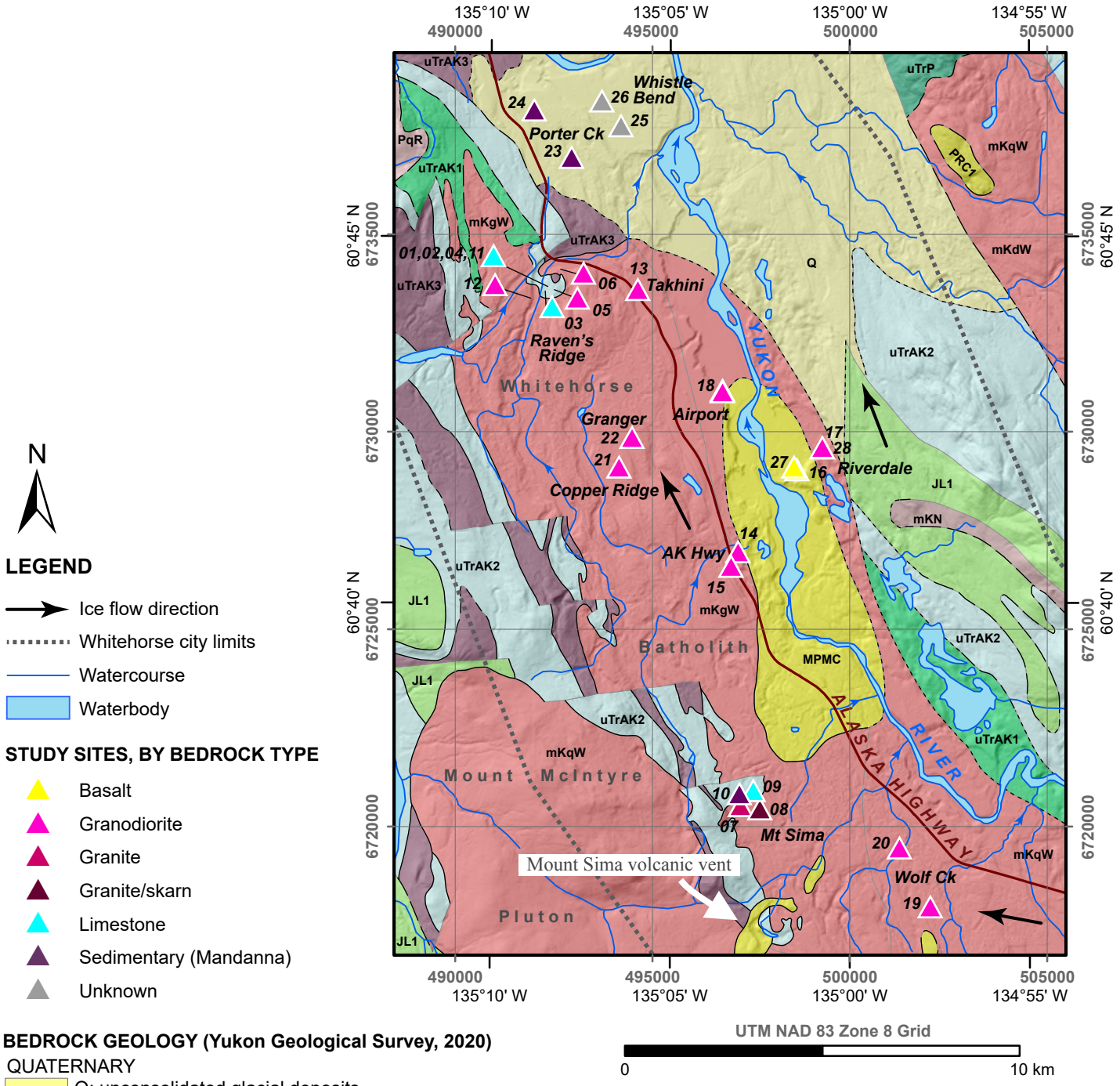

BEDROCK GEOLOGY (Yukon Geological Survey, 2020)

QUATERNARY
- Q: unconsolidated glacial deposits

MIOCENE TO PLIOCENE (LATE TERTIARY)
- MPMC: Miles Canyon basalt

PALEOCENE (EARLY TERTIARY)
- PRC1: Rhyolite Creek rhyolite and dacite
- PqR: Ruby Range Suite granite

MID-CRETACEOUS
- mKqW: Whitehorse Suite monzonite, granite and leucogranite
- mKgW: Whitehorse Suite granodiorite and diorite
- mKdW: Whitehorse Suite diorite
- mKN: Mount Nansen andesite to dacite

UPPER TRIASSIC
- uTrAK1: Casca shale, siltstone, sandstone, limestone
- uTrAK2: Hancock limestone
- uTrAK3: Mandanna sandstone, pebble conglomerate, mudstone
- uTrP: Povoas andesitic basalt flows, breccia, tuff, sandstone, argillite

LOWER AND MIDDLE JURASSIC
- JL1: Richtofen sandstone, siltstone, mudstone, conglomerate

Figure 2. Bedrock geology of the Whitehorse area (Yukon Geological Survey, 2020a). Numbered triangles correspond to study sites (e.g. pink triangle labelled "19" is site 20MK-019).

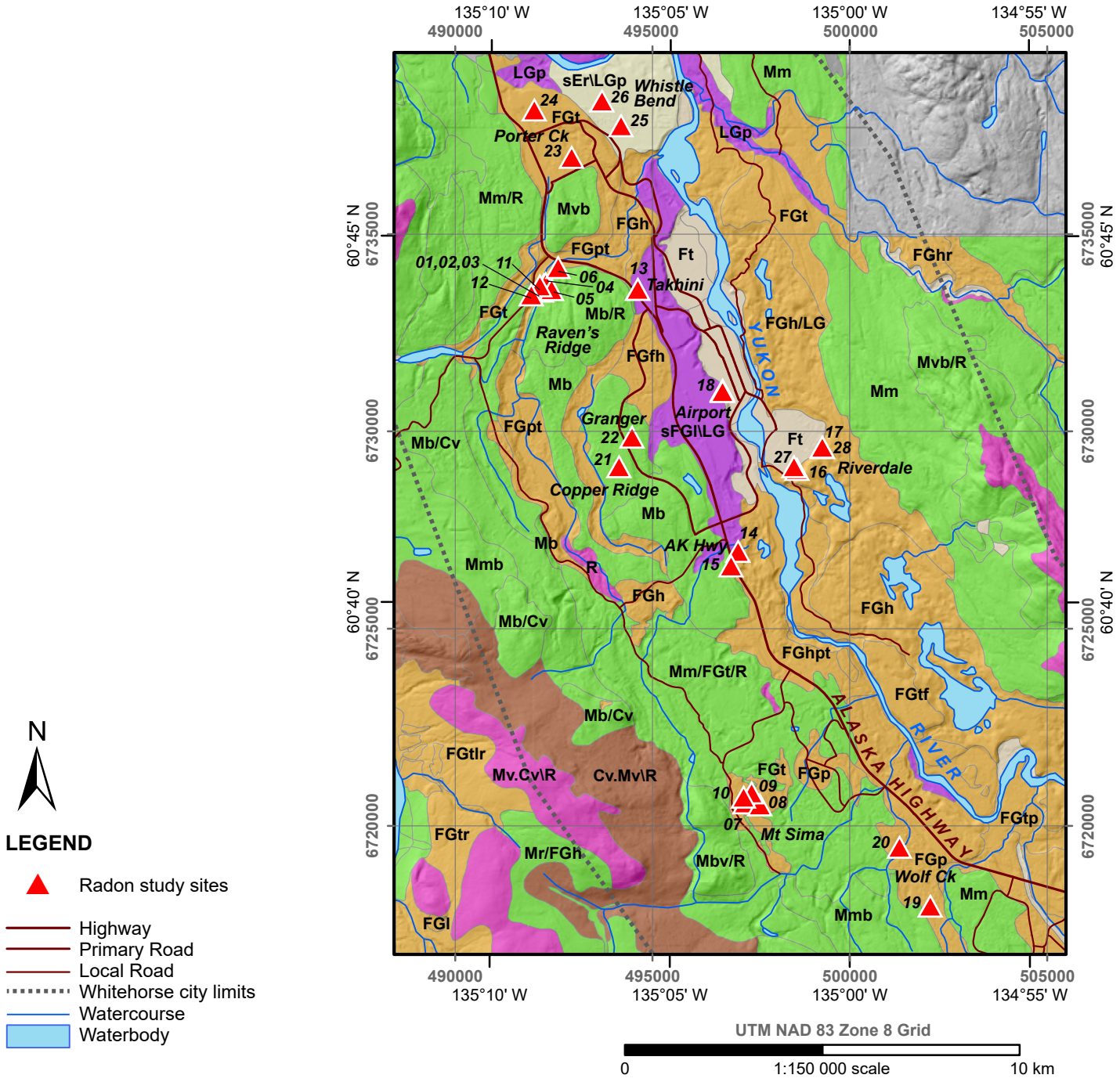

N

LEGEND

- Radon study sites
- Highway
- Primary Road
- Local Road
- Whitehorse city limits
- Watercourse
- Waterbody

SIMPLIFIED SURFICIAL GEOLOGY (modified from Bond, Morison & McKenna, 2005a,b,c)

- F: Fluvial: floodplains (Fp), terraces (Ft), fans (Ff)
- O: Organic
- E: Eolian: sand dunes (sEr), loess (zEv)
- C: Colluvial: veneer (Cv), apron (Ca)
- FG: Glaciofluvial: plain (FGp); terrace (FGt); delta (FGl)
- LG: Glaciolacustrine: plain (LGp)
- M: Moraine (Till): blanket (Mb), veneer (Mv), streamlined (Mm), ridged (Mr)
- R: Bedrock

Figure 3. Surficial geology of the Whitehorse area (Bond et al., 2005a, b, c). Numbered triangles correspond to study sites.

2.2 Radon

2.2.1 Sources of soil radon

Radon-222, the longest-lived isotope of radon, is a product of the uranium decay series, produced only as an alpha-decay daughter of ^{226}Ra ($t_{½}$ = 1602 yr). Uranium occurs naturally, especially in granitic rocks, enriched veins, and ores. Uranium-bearing rocks and minerals in surficial sediment provide a near-surface source for radon. An inert noble gas, radon escapes the host mineral both by diffusion and recoil (Nazaroff, 1992). Radon remains unionized, and is therefore mobile in both air and water, and can be transported to the surface through advection, dissolution in groundwater, diffusion, and passage through faults and fractured bedrock (Fig. 4). At the surface, radon quickly dissipates in the atmosphere, and is therefore not hazardous in outdoor spaces (Government of Canada, 2020).

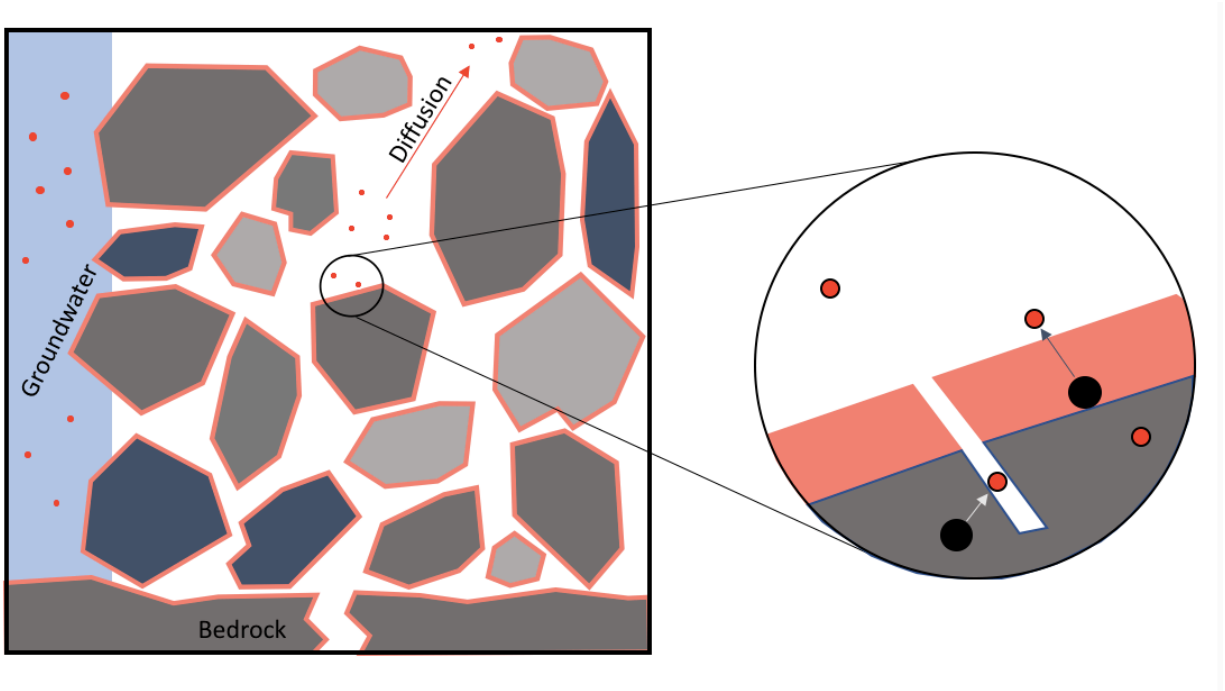

Figure 4 – Radon emanation and transport. Not to scale.
Red dots indicate radon atoms (gaseous), black dots indicate radium (solid). Pink rind on clasts and bedrock indicates area of direct ejection into pore space. Diffusion of radon occurs through clast crystal lattices and along fission tracks (emanation) and between clasts (transport). See Nazaroff (1992) for definitions. Radon is soluble in water and therefore also transported in solution.

2.2.2 Uranium

There are several known occurrences of uranium in the Whitehorse area, such as west of Fish Lake and along the western arm of Bennett Lake (Yukon MINFILE, 2021). The latter is roughly 70 kilometers south of Whitehorse (and therefore up-ice), and is a potential source of uranium in glacial till and derived sediments. The uranium is typically contained in various oxides (e.g. U_3O_8). While free uranium may be dissolved and mobilized in surficial sediment and groundwater, it is likely that the majority of uranium present in Whitehorse-area sediments is bound in minerals. Two common uranium-bearing minerals are apatite (generally $Ca_{10}(PO_4)_6(OH,F,Cl)_2$) and zircon (generally $(Zr_{1-y}, REE_y)(SiO_4)_{1-x}(OH)_{4x-y}$). The lifetime of apatite is relatively shorter than that of zircon, since apatite comminutes more quickly and is more soluble. One might therefore expect zirconium-related uranium to be more evident in the mature sediment types. Uranium may also be present in calcite and other calcium-bearing minerals as a result of substitution of U^{2+} with Ca^{2+}. Whole-rock geochemistry of Whitehorse suite granodiorite reveals that uranium concentration varies from 2.4 to 5.2 ppm (Yukon Geological Survey, 2020b).

2.2.3 Previous radon studies in Yukon

The Yukon Geological Survey undertook the first sampling of radon concentration in sediment in the Yukon at three control sites (20MK-013, 20MK-014, and 20MK-015; Fig 3) from fall 2019 to spring 2020. The present study incorporates these results. In addition to those soil radon measurements, Yukon Housing Corporation has compiled extensive indoor radon testing results from homes in Whitehorse and other Yukon communities for the 2006-2018 period (Fig. 1; Government of Yukon, 2020). Based on data compiled for the Whitehorse area, the highest concentrations of indoor radon occur in Wolf Creek, Canyon Crescent, Pine Ridge and Whitehorse Copper subdivisions. Moderate indoor concentrations (still exceeding the Canadian guideline) are reported in several subdivisions, including Mount Sima, Porter Creek, and Riverdale. The Government of Yukon has also tested schools throughout Yukon and found that radon levels exceed the recommended level in three schools (Government of Yukon, 2018).

3. Field and analytical methods

3.1 Site selection

Sample sites were selected based on the presence of undisturbed uniform surficial sediment, known sediment thickness, and well-constrained surficial stratigraphy (from nearby water well or borehole logs). To achieve uniform bedrock controls, best attempts were made to cluster sample sites away from sediment or bedrock unit boundaries, or known faults. Sites were chosen in representative, well-defined units so that results can be transferred to other areas in Yukon.

3.2 Sampling protocol

In this thesis, the term *soil* will be used in the engineering sense denoting unconsolidated particulate mineral and organic matter, and should not be taken to mean the weathered upper portion of a sedimentary deposit. The Geological Survey of Canada protocol for measuring radon in soils (Friske *et al*., 2010) was closely followed (Fig. 5). In particular, soil gas radon concentration was measured at five points within the 10 x 10 m area of a site (Fig. 6) and revisited at least once, for a minimum of ten measurements per site during the summer season. Revisits were separated by at least one day. Radon results averaged for each site therefore provides average concentration over both time and space. An example of a sampling site is provided in Figure 7. The three control sites (20MK-013, 20MK-014, and 20MK-015) were sampled monthly for nine months and their data are incorporated into this study. The measured concentration of radon in sediment was compared to a range of site characteristics to assess their effect on radon concentration. These suspected controls include: bedrock and surficial sediment geochemistry, depth to bedrock, surficial sediment grain size distribution, sediment maturity, and soil moisture. See Appendix 1 for full descriptions of each site, including environmental characteristics such as vegetation and soil profile.

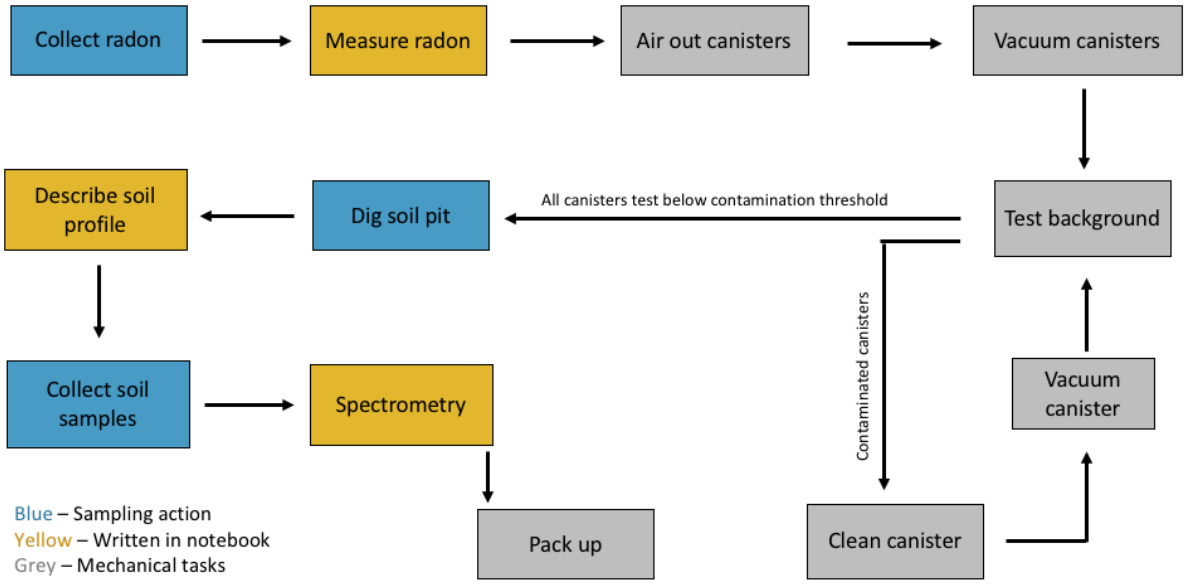

Figure 5 – Flowchart of sampling tasks during first visit to site. Based on protocol from Friske *et al.* 2010.

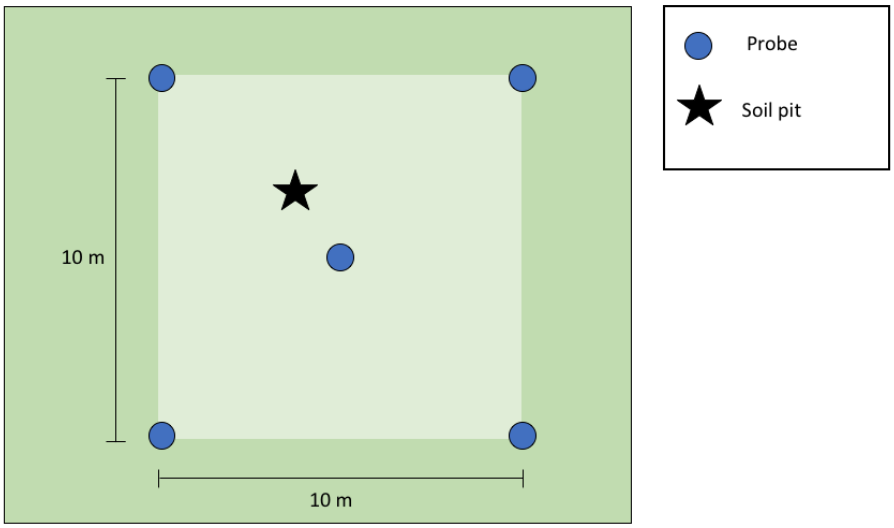

Figure 6 – Typical geometry of a sample site, with probes in corners and center of 10x10 m grid, and soil pit near the center probe. Exact placement of soil pit varied depending on position of trees, boulders, and other obstructions.

Figure 7 – Photograph of sampling site 20MK-010 on June 18, 2020.
Glaciofluvial gravel overlying Mandanna member of the Aksala Formation (sandstone and conglomerate). Three bags of sediment, from left to right, for clast lithology/geochemical analysis, matrix geochemistry, and grain size distribution. The spectrometer case is visible in top right and a probe flagged with orange tape can be seen in the top left.

3.3 Radon collection

To ensure consistency with methodology used elsewhere in Canada, I followed the sampling protocols outlined by Friske *et al.* (2010), and used the same equipment and instruments described therein (borrowed from Geological Survey of Canada-Ottawa). Soil gas was collected from each site by inserting a piece of narrow metal pipe (hereafter referred to as a "probe") to a depth of 60 cm. This is the depth recommended by Friske *et al*. (2010) and aims to sample a soil's C-horizon. A sharp steel point was placed at the groundward end of the probe, which was then hammered into the sediment with a mallet. A "punch rod," thinner and longer than the probe, was then tapped through the probe, pushing the tip roughly 5 cm deeper and creating an air cavity at the end of the probe. A 150 ml syringe was used to extract soil gas (Fig. 8). The first 150 ml of gas were purged to clear the probe of any atmospheric air, and the second volume was used to fill an evacuated ionization chamber (Fig. 9). Uncertainty in volume is estimated to be ± 10 ml (1σ). Concentrations were measured *in situ* using an ERM-3 Soil Radon Meter manufactured by Radon v.o.s. of Prague, using the protocol in the accompanying manual

(included in Friske *et al.* 2010). Some canisters did not fill completely, due either to low soil permeability and incomplete syringe fill, or to insufficient vacuum in the canister. In these cases the following error correction was applied according to the ERM-3 radon meter manual:

$$C_{cor} = C_{meas} \text{ x } \frac{150}{V_{in}} \quad (1)$$

where C_{cor} is the corrected concentration measurement in kBq m^{-3}, C_{meas} is the concentration reported by the radon meter in kBq m^{-3}, and V_{in} is volume of soil gas extracted via syringe in ml.

Figure 8 – Soil gas extraction using 150 ml syringe. Red rubber tube connects directly to valve on ionization chamber. Probe flagged with orange tape.

Figure 9 – IK-250 ionization chamber for radon concentration measurement, 250 ml capacity. Serial number is red, electrodes are brass pin at left and silver pin in central cylinder. Valve at right (knob above protruding tube).

3.4 Field collection of environmental data

Additional geological and environmental information deemed relevant to radon concentration was collected from each site. A >60 cm soil pit was dug by shovel within a few meters of the central soil gas probe, and four sediment samples were collected from a depth of 60 cm (same depth as probe tips) for the following analysis: geochemistry of the matrix and representative clasts, sediment grain size, clast lithology on 50–100 pebbles averaging 5 cm long axis, and soil moisture on 250 ml of sediment. If fewer than 50 clasts were available in the sediment, I collected as many as possible. The following sites had no clasts present: 20MK-006, 007, 11, 012, 013, 018, 025, 026 and 027. Gamma ray spectrometry was conducted at each probe and soil pit to measure dose rate, potassium, equivalent uranium, and equivalent thorium. A wandering gamma ray survey of the site ensured that no areas produced anomalous levels of radioactivity (e.g., due to a granite boulder). The weathered soil profile was described (horizon type and thickness, surficial sediment classification, and evidence of disturbance) as well as local meteorological conditions (pressure, air temperature, humidity and wind) at the time of each sampling, and a general description of the site including topography and vegetation was made on the first visit (Appendix 1). Where accessible, bedrock samples for geochemical analyses were collected as close to the site location as possible.

3.5 Analytical methods

3.5.1 Radon gas concentration

All measured data are reported including any perceived anomalies. Mean radon concentration was calculated by first taking the average and standard deviation of all samples at a site, then removing measurements one standard deviation or greater from the mean (these are considered outliers) to determine if the standard deviation improved significantly, and finally recalculating mean and standard deviation of radon concentration with outliers removed. Weighted means were calculated according to the following formula:

$$W = \frac{\sum_{i=1}^{n} w_i x_i}{\sum_{i=1}^{n} w_i} \quad (2)$$

where W is the weighted mean, x is a mean calculated by the above method, and $w_i = (1 - CoV)$. CoV is the coefficient of variation (standard deviation divided by mean).

3.5.2 Grain size distribution and sorting

Approximately 1 kg of matrix sample was collected from each soil pit to determine grain size distribution. Clasts larger than 5 cm were removed by hand, as they are not considered part of the matrix. Grain size distribution was determined by Pacific Soil Analysis Inc. (Richmond, British Columbia) using sieve separation and a hydrometer. Two sets of sieve sizes were used: 3 inches, 19 mm, 8 mm, 4 mm, and 2 mm; and #10 (2 mm), #18 (1 mm), #35 (500 micron), #60 250 micron), #140 (106 micron), 53 micron, and 2 micron. GRADISTAT Excel software (Blott and Pye, 2001) was used to calculate the degree of sorting based on the sieving data. This software returns arithmetic, geometric and logarithmic sorting statistics, as well as textural description based on the Folk and Ward classification. The sorting statistics reported here are all geometric.

3.5.3 Soil moisture

Immediately before the radon gas measurement at a given site, soil moisture was determined by collecting a representative sample (roughly 0.5 kg of sediment) in a waterproof container from a depth of 60 cm in the soil pit. The sample was collected as soon as this depth was reached, to minimize evaporation upon exposure to the atmosphere. The sediment was weighed in the field (m_w) using a Starfrit High Precision Pocket Scale. The same day, samples were baked at 100°C for one hour, cooled, and reweighed (m_d), and the difference in mass was used to estimate soil moisture (SM, %) according to

$$SM = \frac{m_w - m_d}{m_w} \; x \; 100. \qquad (3)$$

3.5.4 Geochemistry

To investigate relationships between radon and the chemical properties of sediment matrix and clasts within the sediment, targeted samples were analyzed for ^{222}Rn parents and for elements indicative of ^{222}Rn source minerals. Approximately 0.5 kg of sediment matrix from each site, as well as select representative pebble-sized clasts, were analyzed for major, minor,

and other selected elements, and for loss on ignition. Whole rock geochemistry was completed at ALS Global (North Vancouver, British Columbia) using their complete characterization package. This included sample preparation and screening of the samples to 180 μm and the following analytical suite: whole rock by fusion/XRF, base metal by 4-acid digestion, loss on ignition for XRF, lithium borate fusion ICP-MS, and up to 34 elements by ICP-MS, as well as total carbon and total sulphur by IR spectroscopy. In addition to assessing U-series elemental abundances, analysis of the majors enabled the use of a chemical index of alteration (e.g. Nesbitt *et al*., 1982) to help quantify sediment maturity—a potential controlling factor for soil radon activity. No reference materials were submitted with the samples, however a duplicate sample of site 20MK-014 matrix was submitted. Reported variation was within one percent, suggesting high reproducibility.

3.5.5 Statistical analysis

To elucidate the controlling factors on radon concentration in surficial sediment, I used the PAST software package developed by Øyvind Hammer at the University of Oslo (Hammer *et al*., 2001). I used this software to conduct univariate and multivariate statistical analysis on chemical and physical data, revealing the strength of correlation between different factors. Specifically, I used PAST to compute univariate correlation and multivariate principal component analysis. Determining the relative influence of various factors (e.g. silt and clay content of matrix, uranium content of matrix, depth to bedrock) on radon concentration allows for the testing of my hypotheses.

4. Results

4.1 Soil radon gas measurements

During the 2020 field season, 328 soil gas samples from 30 sites throughout the Whitehorse area were tested for radon concentration. Individual radon concentrations ranged from 0 to 68.1 kBq m^{-3}. The majority of sites (17 of 30) overlie granodiorite, while six overlie limestone, three overlie clastic sedimentary rocks, two overlie basalt, and two overlie unmapped bedrock (Fig. 2, 10, Appendix 1). Depth to bedrock (typically determined from water well drill logs) ranges from 1.5 m to greater than 100 m (the deepest being in Whistle Bend where glaciogenic sediments have not been drilled to bedrock). Twelve of the 30 sites are in glaciofluvial deposits, while six are in till, five are in fluvial sediments, two are in glaciolacustrine deposits, one is in eolian sediment, and two are in bedrock. Two sites in diamicton remobilized downhill from a mapped till deposit (Bond *et al*., 2005a–c) onto a terrace are classified in this thesis as "colluviated till" because their genetic link to the tills is likely more useful when interpreting the results than simply "reworked diamicton". The grain size distribution of these samples is expected to be different from other till samples, but the clast lithology and some aspects of the geochemistry will be similar. Soil moisture varies from 2 to 14% by weight. Coefficients of variation of the mean concentration of Rn-222 range from 2 to 86%, with an average coefficient of variation of 27%. Variation is highest in silt and gravel units (average 62 and 29% respectively) and lowest in till and sand units (average 19 and 17% respectively). The mean concentrations of radon in three prominent sediment types sampled in this study, calculated from data collected over the entire field season and weighted according to the coefficient of variation at each site, are 7.4 kBq m^{-3} for sand, 8.3 kBq m^{-3} for gravel and 16.0 kBq m^{-3} for till.

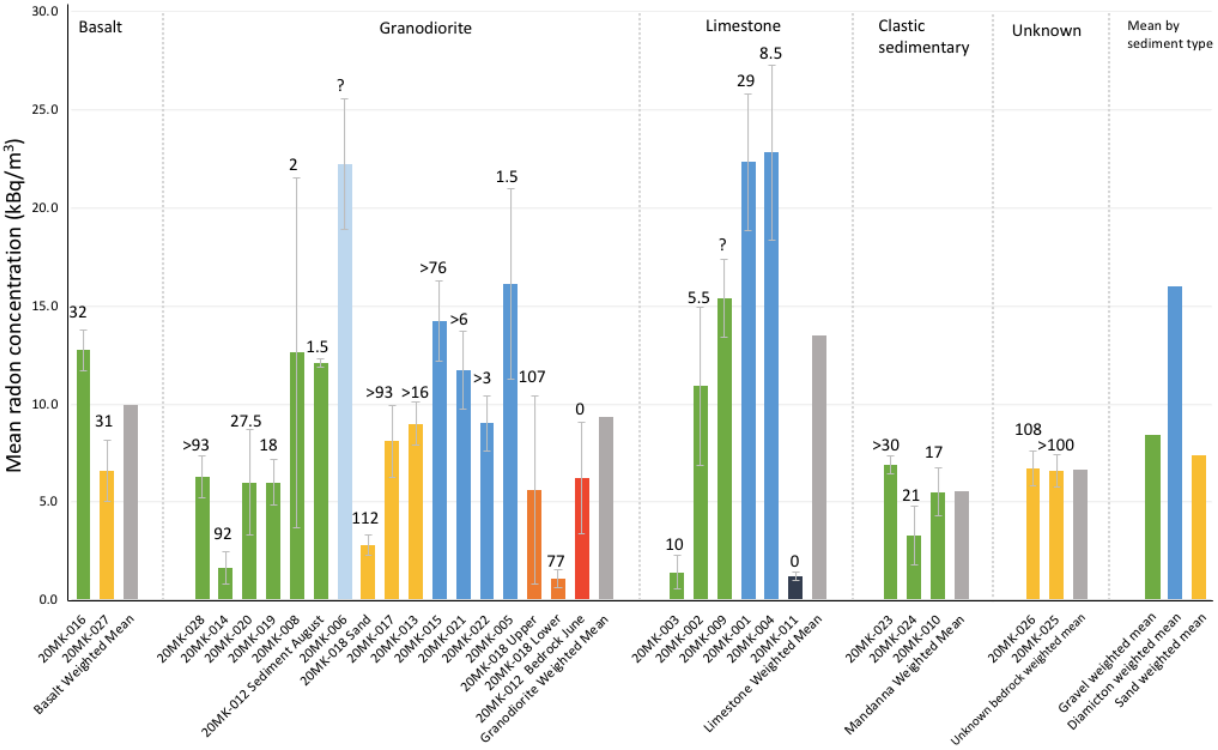

Figure 10 – Mean soil gas radon concentration (min. 10 measurements) sorted by sediment and bedrock type. Concentration grouped by underlying bedrock type, and coloured according to sediment textural classification. Within each bedrock-surficial sediment class, concentrations are sorted by depth to bedrock (represented as data labels, in metres). Means weighted by coefficient of variation were also calculated for each bedrock type (grey bars) and major surficial sediment texture (3 bars at far right). Two sites with high radon concentration are omitted to avoid skewing the graph: colluviated till overlying granite (20MK-007) and granodiorite saprolite (20MK-012), with mean radon concentrations of 45.6 and 55 kBq m^{-3} respectively.

4.2 Seasonality

To determine if soil radon concentration varies seasonally, three sites (20MK-013, 20MK-014, and 20MK-015) were monitored monthly from August 2019 to August 2020, with a gap from February to April 2020 (Fig. 11). These sites were chosen as representative of sand, gravel, and diamicton respectively. Soil radon measurements from August 2019 to January 2020 were collected by the Yukon Geological Survey. While more data over multiple years is needed

to provide reproducibility in these results, the data from each of the three sediment types appear to exhibit different seasonal distributions. In till, the measured mean soil radon concentration is higher during the summer months, while in gravel it is measurably lower in summer. Seasonal variation is less significant in sand, however December and January had the highest measured concentrations, suggesting a trend similar to that observed in gravel. From May to August 2020 (the main sampling period of this study), the mean monthly values for gravel and sand are within 1σ error of their mean and overlap, but are significantly more variable from October to January. On the other hand, at the diamicton site the months with consistent data (overlapping 1σ error) were September to January.

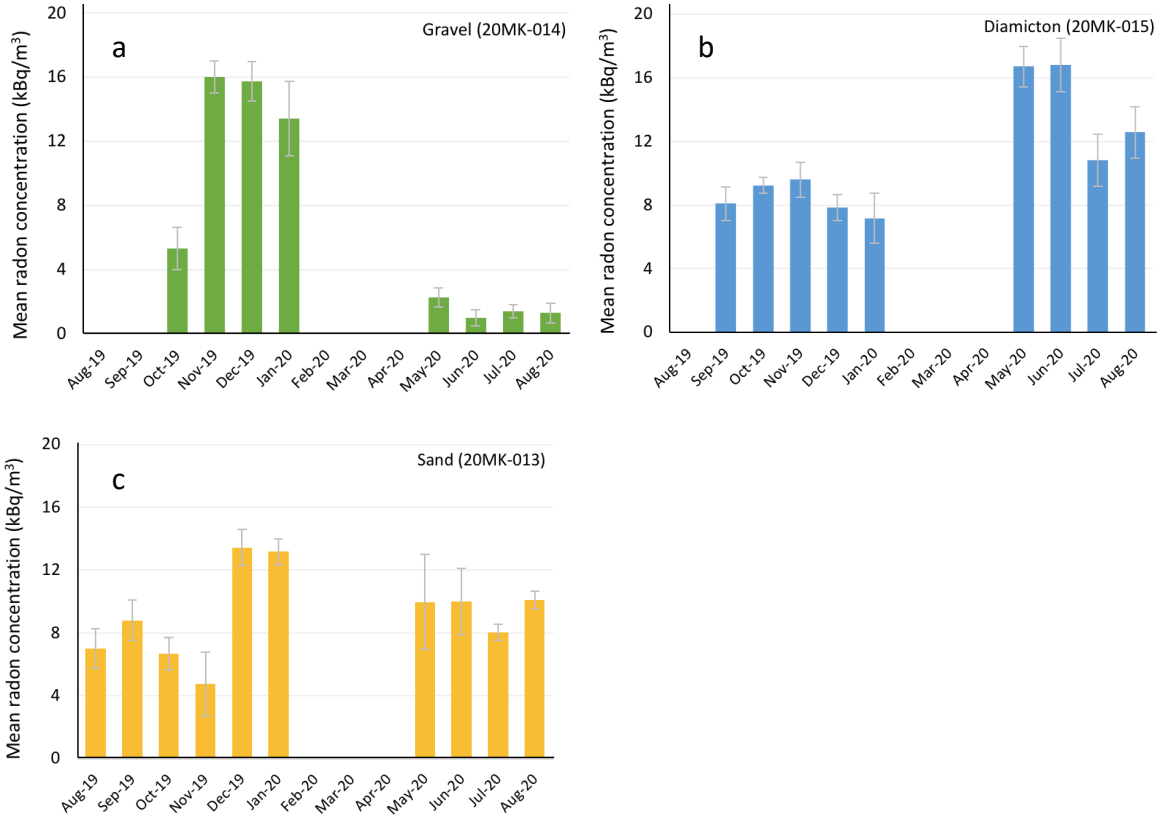

Figure 11 – Mean soil gas radon concentration at three long-term monitoring control sites. Data from glaciofluvial gravel (a), lodgement till (b), and fluvial sand (c) are plotted individually. Error bars are 1σ. Note that data are missing from February through April due to adverse winter sampling conditions and onset of global pandemic.

4.3 Bedrock and surficial sediment type

I grouped mean soil radon concentrations according to the site's bedrock and surficial sediment type (Fig. 10) and calculated the CoV-weighted mean concentration for each bedrock type across surficial sediment types (grey bars, Fig. 10). Out of bedrock type, depth to bedrock, and surficial sediment type, the most influential control on radon concentration is surficial sediment type. Its relative importance will be evaluated statistically in §4.9. The weighted means for sites overlying basalt and granodiorite are nearly identical (9.9 and 9.4 kBq m^{-3} respectively), and slightly higher for sites overlying limestone (13.5 kBq m^{-3}). Diamicton has relatively high radon concentration, while sand is generally low and gravel is intermediate. The CoV-weighted mean concentration of radon in till is 16.0 kBq m^{-3}, while gravel and sand have similar weighted means with 8.3 kBq m^{-3} in gravel and 7.4 kBq m^{-3} in sand. There is a possible bimodality in gravel concentration, which may be related to sorting or to clast proportion. There does not appear to be a relationship between radon concentration and the thickness of sediment cover (i.e. depth to bedrock) (see Fig. 10 data labels). If neither depth to bedrock nor bedrock type explain the apparent variance in radon concentration, it is possible that other factors, including geochemistry, sediment properties, or soil moisture are more important controls.

4.4 Grain size distribution

In order to determine if a relationship exists between grain size distribution of sediment cover and radon concentration, I compared mean radon concentration from each site to the fraction of matrix that is less than 53 μm in diameter (i.e., silt and clay; Fig. 12). The fine fraction was selected in part because silts and clays can reduce the permeability of the sediment, a characteristic I was unable to measure directly. Complete grain size distribution results are provided in Appendix 2. The tills (classified texturally as diamicton), along with the colluviated tills that were reworked and deposited on a terrace, show the highest fraction of silt and clay in the matrix. The moderately sorted to very poorly sorted gravels consistently have relatively low abundances of fines, while sand displays a bimodal distribution of matrix grain size that is interpreted to be related to genesis (i.e. eolian versus fluvial/glaciofluvial origins, discussed further in §4.6). Results of the grain size analyses suggest a positive correlation between radon

concentration and fraction of the matrix that is <53 µm diameter, with a coefficient of determination $R^2 = 0.59$. This is one of the strongest correlations of any that I tested.

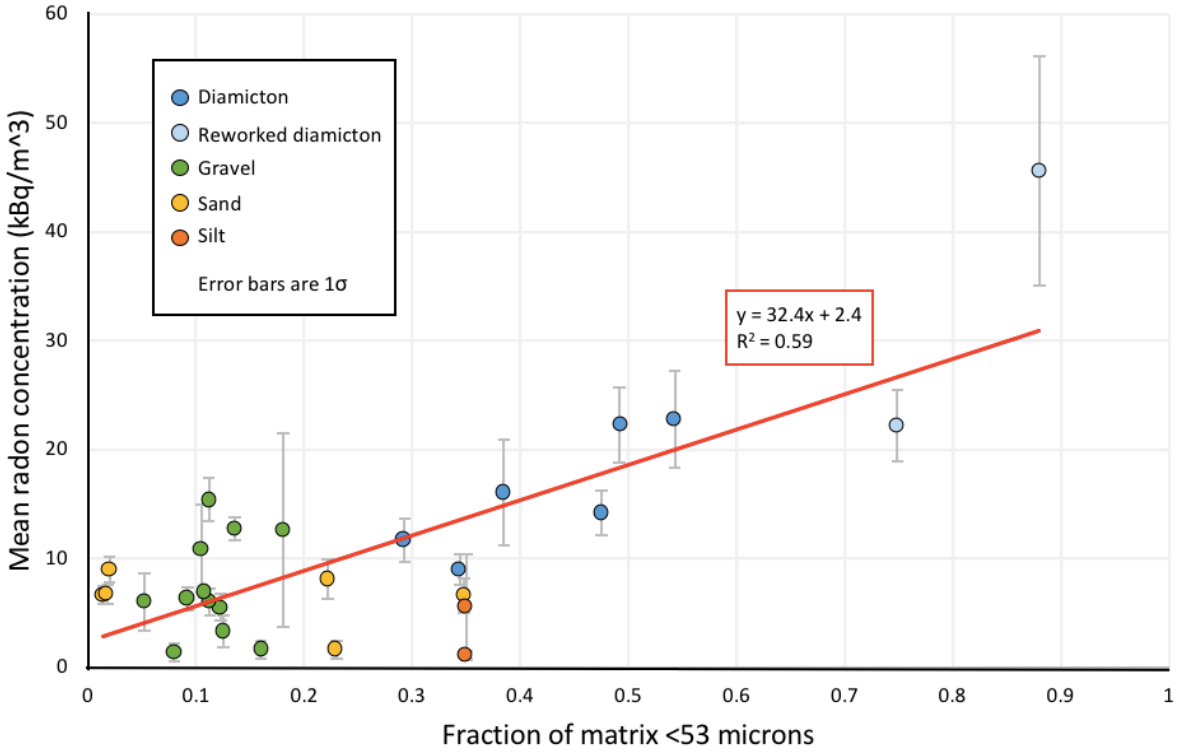

Figure 12 – Mean radon concentration compared to the fraction of silt and clay in the sediment matrix. Data points are coloured according to surficial sediment type. Glaciolacustrine matrix samples were not collected so grain size distribution from Brideau *et al*. (2011) at a nearby sample location is used as a proxy for the two silt samples (orange). Note that the colluviated tills have a higher fraction of fines than the unreworked till, as expected, and that the effect of the colluviated tills on radon concentration seems consistent with the more general relation between fine fraction and radon.

4.5 Sorting

I also compared mean radon concentration at each site to the sorting of the matrix from the soil pit sample (Fig. 13). To do this, a geometric sorting statistic (σ) was calculated using GRADISTAT version 4.0 (Blott and Pye, 2001). No significant relationship was observed between radon concentration and matrix sorting. Since only the grain size distribution of the *matrix* of each sample was analyzed, the sorting reported here does not reflect the overall sorting of the sediment (i.e. fine fraction and sands and pebbles). For example, till is typically more poorly sorted than gravel, however some till samples had relatively well-sorted and unimodal

matrices. Descriptive classifications of the matrix, based on the schema of both Wentworth (1922) and Folk and Ward (1957), are reported in Table 1. Although it does not represent the overall sorting of the sediment, matrix sorting may be used as a rough proxy for permeability, since uniform grain size increases permeability (cf §4.7 on Moisture).

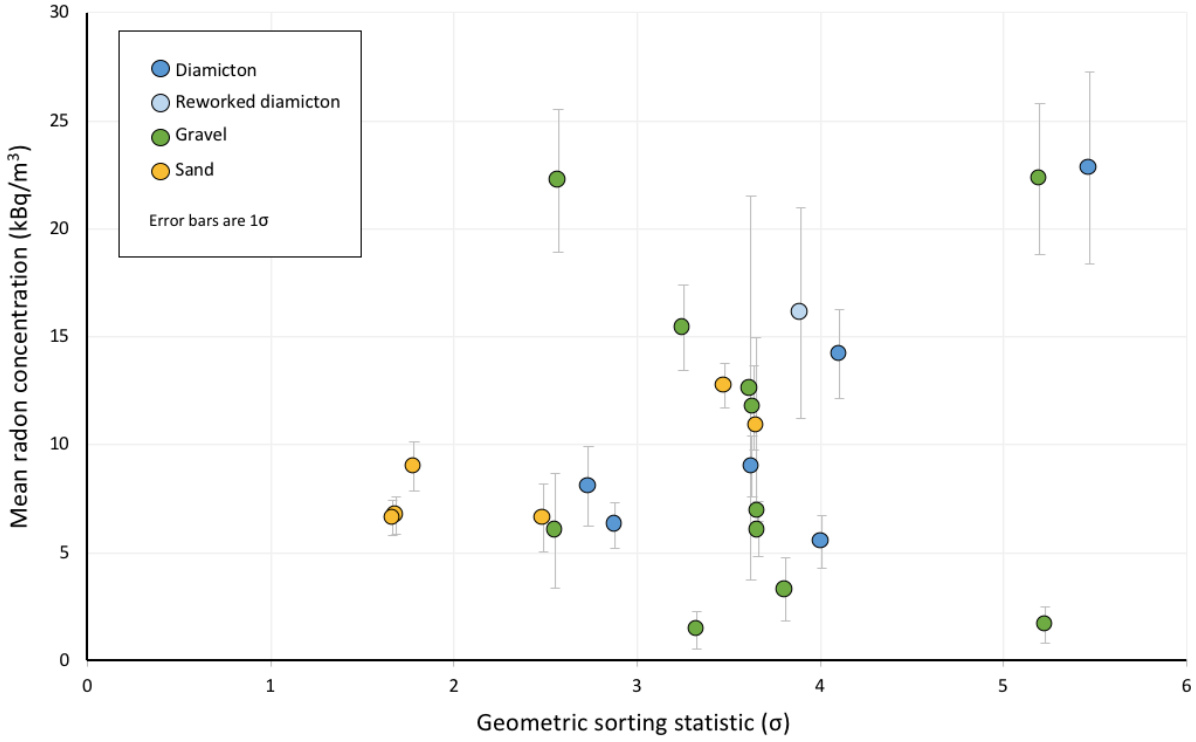

Figure 13 – Mean radon concentration compared to matrix sorting statistic as calculated by GRADISTAT Excel package (Blott and Pye, 2001). Greater values of geometric sorting statistic indicate poorer sorting of the matrix .

Table 1 – Description of matrix grain size, by textural group (based on Wentworth), geometric sorting statistic, and Folk and Ward classification. Note that grains 2-4 mm are considered "very fine gravel" by the Wentworth scale, and therefore several fine-grained sites (eg. 20MK-006, 20MK-025, and 20MK-027) are described as "gravelly" in the second column.

SITE	TEXTURAL GROUP	SIGMA (GEO.)	FOLK&WARD MEAN	FOLK&WARD SORTING
20MK-001	Gravelly Muddy Sand (diamicton)	5.20	Fine Sand	Very Poorly Sorted
20MK-002	Gravelly Sand	3.65	Very Coarse Sand	Poorly Sorted
20MK-003	Sandy Gravel	3.33	Very Coarse Sand	Poorly Sorted
20MK-004	Slightly Gravelly Muddy Sand (diamicton)	5.47	Very Fine Sand	Very Poorly Sorted
20MK-005	Gravelly Muddy Sand (diamicton)	3.89	Fine Sand	Poorly Sorted
20MK-006	Slightly Gravelly Muddy Sand	2.57	Very Fine Sand	Poorly Sorted
20MK-007	Slightly Gravelly Muddy Sand	2.14	Very Fine Sand	Moderately Sorted
20MK-008	Gravelly Sand	3.62	Medium Sand	Poorly Sorted
20MK-009	Gravelly Sand	3.25	Coarse Sand	Poorly Sorted
20MK-010	Sandy Gravel	4.01	Very Coarse Sand	Poorly Sorted
20MK-013	Sand	1.78	Medium Sand	Moderately Sorted
20MK-014	Gravelly Muddy Sand	5.23	Coarse Sand	Very Poorly Sorted
20MK-015	Slightly Gravelly Muddy Sand (diamicton)	4.11	Fine Sand	Very Poorly Sorted
20MK-016	Gravelly Sand	3.48	Medium Sand	Poorly Sorted
20MK-017	Slightly Gravelly Muddy Sand	2.74	Fine Sand	Poorly Sorted
20MK-019	Gravelly Sand	3.66	Very Coarse Sand	Poorly Sorted
20MK-020	Gravelly Sand	2.55	Coarse Sand	Poorly Sorted
20MK-021	Gravelly Muddy Sand (diamicton)	3.64	Medium Sand	Poorly Sorted
20MK-022	Gravelly Muddy Sand (diamicton)	3.63	Medium Sand	Poorly Sorted
20MK-023	Gravelly Sand	3.66	Very Coarse Sand	Poorly Sorted
20MK-024	Gravelly Sand	3.81	Coarse Sand	Poorly Sorted
20MK-025	Slightly Gravelly Sand	1.66	Coarse Sand	Moderately Well Sorted
20MK-026	Sand	1.68	Coarse Sand	Moderately Well Sorted
20MK-027	Slightly Gravelly Muddy Sand	2.49	Fine Sand	Poorly Sorted
20MK-028	Slightly Gravelly Sand	2.88	Coarse Sand	Poorly Sorted

4.6 Maturity

Maturity, or derivative degree of bedrock, may be a control on radon concentration. My study area encompasses a wide range of sediment types, and I would expect the least weathered or comminuted sediment (e.g. tills) to have a higher abundance of uranium-bearing minerals such as apatite, and the more mature sediments (e.g. the quartz-rich eolian sands) to have a lower abundance. Neither optical nor modal mineralogy assessment of uranium-bearing minerals was attempted, since geochemical analysis of clasts and matrices (§4.8) provides a more precise means of evaluating the effect of sediment maturation on radon concentration. I took three approaches to determine the maturity of the sediments that I sampled, one qualitative and two quantitative.

Qualitatively, I classified sediments (in order from least to most mature) as till, glaciofluvial sand and gravel, fluvial gravel and sand, glaciolacustrine silt, and eolian sand, then compared the CoV-weighted mean radon concentrations of each sediment maturity class (Fig. 14). These classifications were based on surficial mapping by Bond *et al*. (2005a-c) and direct observation of sediment characteristics in soil pits (60 cm depth). Generally, mean radon concentration decreases with inferred sediment maturity, however not uniformly. The weighted means of glaciofluvial and fluvial sediments are almost identical, as expected. Robust statistical analysis is not possible, since the spacing of the points along the x-axis is controlled entirely by the number of samples in each sediment type (an artifact of the site choices with no bearing on abundance or maturity of these sediment types). Though no rigorous comparison is possible, this qualitative approach provides an approximate means of evaluating the effect of the mineralogical composition at a given site.

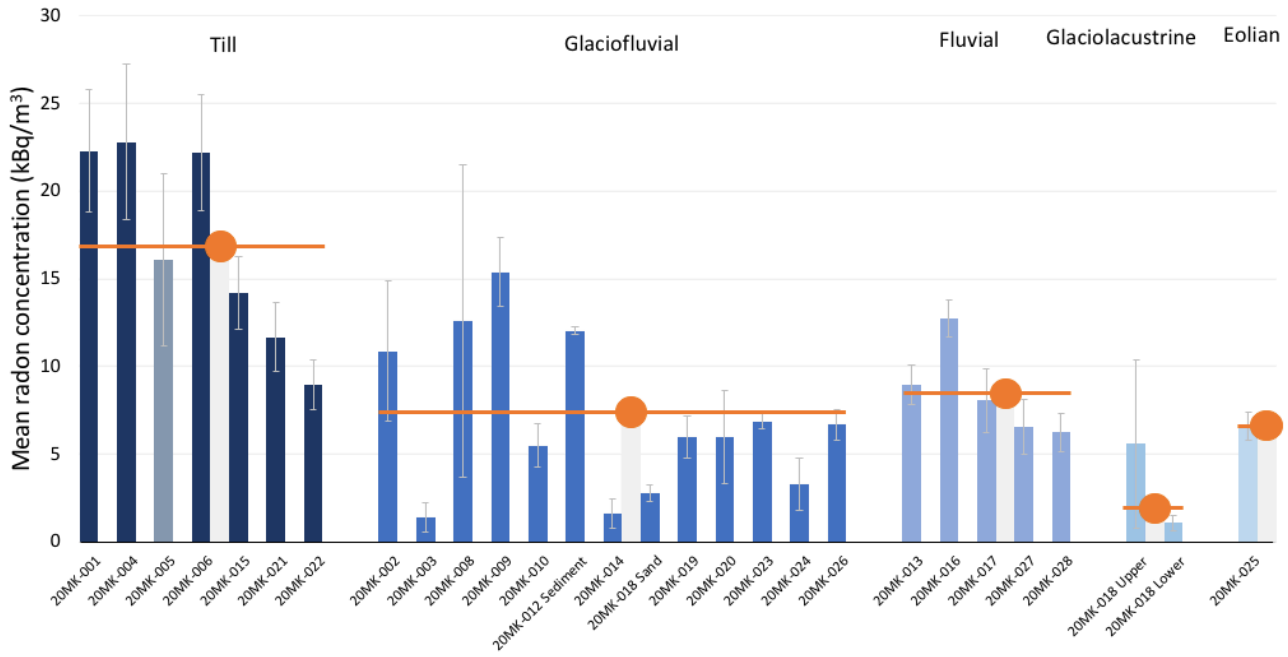

Figure 14 – Surficial sediment classified by maturity, or degree of modification from protolith. Since till is the most directly derived from bedrock, it is at far left, followed by glaciofluvial, fluvial, glaciolacustrine, and eolian sediments. Note the colluviated till sample third from the left (pale bar) and that reworking (i.e., increase of maturity) has not had any appreciable effect on radon concentration. The average of each group is plotted as a single orange point. Error bars are 1σ. Not included in the graph to avoid skewing is 20MK-012, a saprolite site with mean radon concentration of 55 kBq m^{-3}. Since saprolite is more proximate to bedrock than till, this sample supports the overall trend of decreasing radon concentration with increasing maturity.

Quantitatively, I employed the chemical index of alteration (CIA) proposed by Nesbitt *et al*. (1982). This index is essentially the ratio of sediment aluminum concentration to the sum of aluminum, potassium, sodium, and calcium sediment concentrations. Since Nesbitt *et al*.'s CIA was developed to measure the different degrees of weathering of a single (crystalline) bedrock unit, I modified it slightly. Five sites overlying limestone bedrock were removed from the comparison as they might display calcium concentrations much higher than expected, and thereby skew the index. However, basalt was included. I also normalized all terms of the index to titanium concentration, in an attempt to compare across lithology types. Other exclusions and other methods to normalize the dataset were considered, however this approached seemed the most geologically reasonable (Fig. 15). There may be a slight negative correlation between the radon concentration and my modified CIA. It is important to note, however, that the CIA does not correspond to my qualitative classifications of maturity based on sediment type (see data

point colouring), and this may indicate that neither sediment type (sediment genesis) nor CIA are wholly reliable and that the multiple-maturity index approach used here may be beneficial.

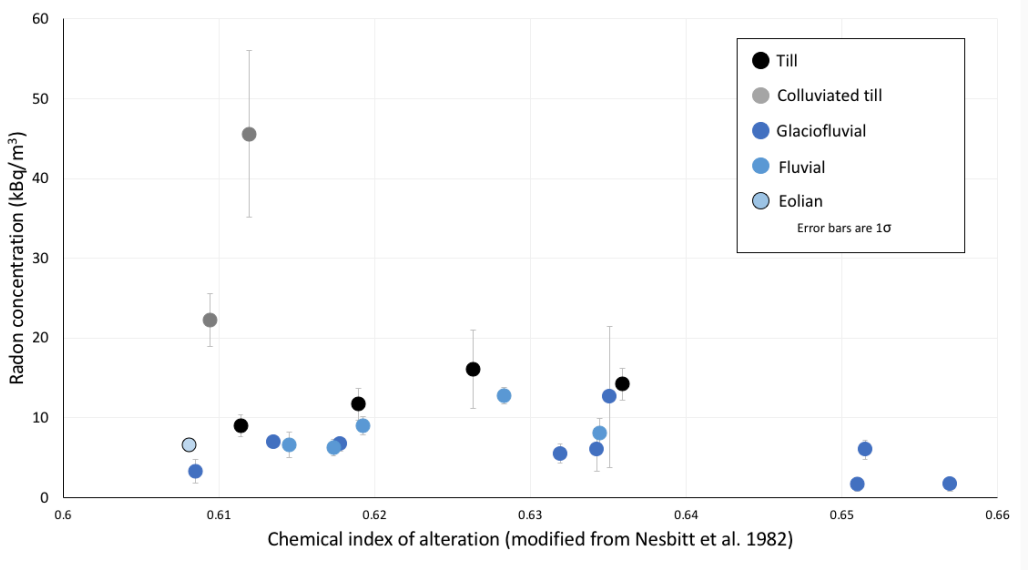

Figure 15 – Mean radon concentration compared to chemical index of alteration. Index developed by Nesbitt *et al.* (1982) and modified for this paper. Larger values of the CIA indicate greater maturity. Specifically, limestone samples were removed to eliminate skewing caused by high non-silicate concentrations of calcium, and all concentrations normalized with respect to titanium concentration to control for lithology. Note one sample lies outside of the graph axes chosen above: glaciolacustrine sample with radon concentration of 1.1 kBq m^{-3} and chemical index of alteration of 0.53.

In summary, neither of the quantitative approaches I tested reproduce my qualitative classification of sediment maturity. These quantitative assessments reflect the composition of only a small aliquot of matrix collected from the base of each soil pit, and since the qualitative classification was based on both published maps (Bond *et al.*, 2005a,b,c) and field observations, it (Fig. 14) may be more representative than the geochemical indices (Fig. 15).

4.7 Moisture

To determine the effect of sediment water content on radon concentration, I measured the mass difference of a dried sample from each soil pit, and compared this estimate of sediment moisture to radon concentration from that site. Previous work (e.g. Thu *et al.*, 2020; Sakoda *et al.* 2010) suggests that radon concentration increases with water content. The effect of moisture on radon is thought to be greater with smaller grain sizes. This is likely because water blocks pore spaces in sediment, preventing the diffusion of radon and concentrating it in unsaturated pore

spaces. A positive correlation between moisture and mean radon concentration is observed with a coefficient of determination $R^2 = 0.39$ (Fig. 16a).

A positive overall trend also exists within each sediment type (Fig. 16b). The coefficient of determination of sand is $R^2 = 0.99$, due perhaps to its relatively uniform porosity and permeability. However, the dependence of radon concentration on moisture in sand is also the lowest (shallowest slope). Furthermore, this trend is based on few points and may not reflect the behavior of sand more generally. Radon is the most variable with respect to moisture in gravel, despite the narrow range of measured moisture contents. The trendline between radon and gravel is steepest but has a low coefficient of determination $R^2 = 0.29$ (Fig. 16b). Till has a coefficient of determination $R^2 = 0.44$, with the widest observed range of moisture content and a slope that is statistically indistinguishable from that of gravel, possibly owing to the weak correlations.

Variation in soil moisture may be caused by differences in the timing and amount of rainfall before each measurement, shallow ground water effects, wind strength (affecting evaporation and advection in the upper 60 cm), soil temperature, vegetation, slope, saturation of soil, and the holding capacity of the sediment. Sediments such as diamictons contain more silt and clay (Fig. 12) and may hold more water than more permeable sands and gravels (see Fig. 16b), which may in turn affect radon concentration. Note that the trendlines in Figure 16a do not take into account the uncertainties of each measurement, and are in some cases heavily affected by a single data point (e.g., rightmost point in Fig. 16a). The actual trends may therefore be less pronounced.

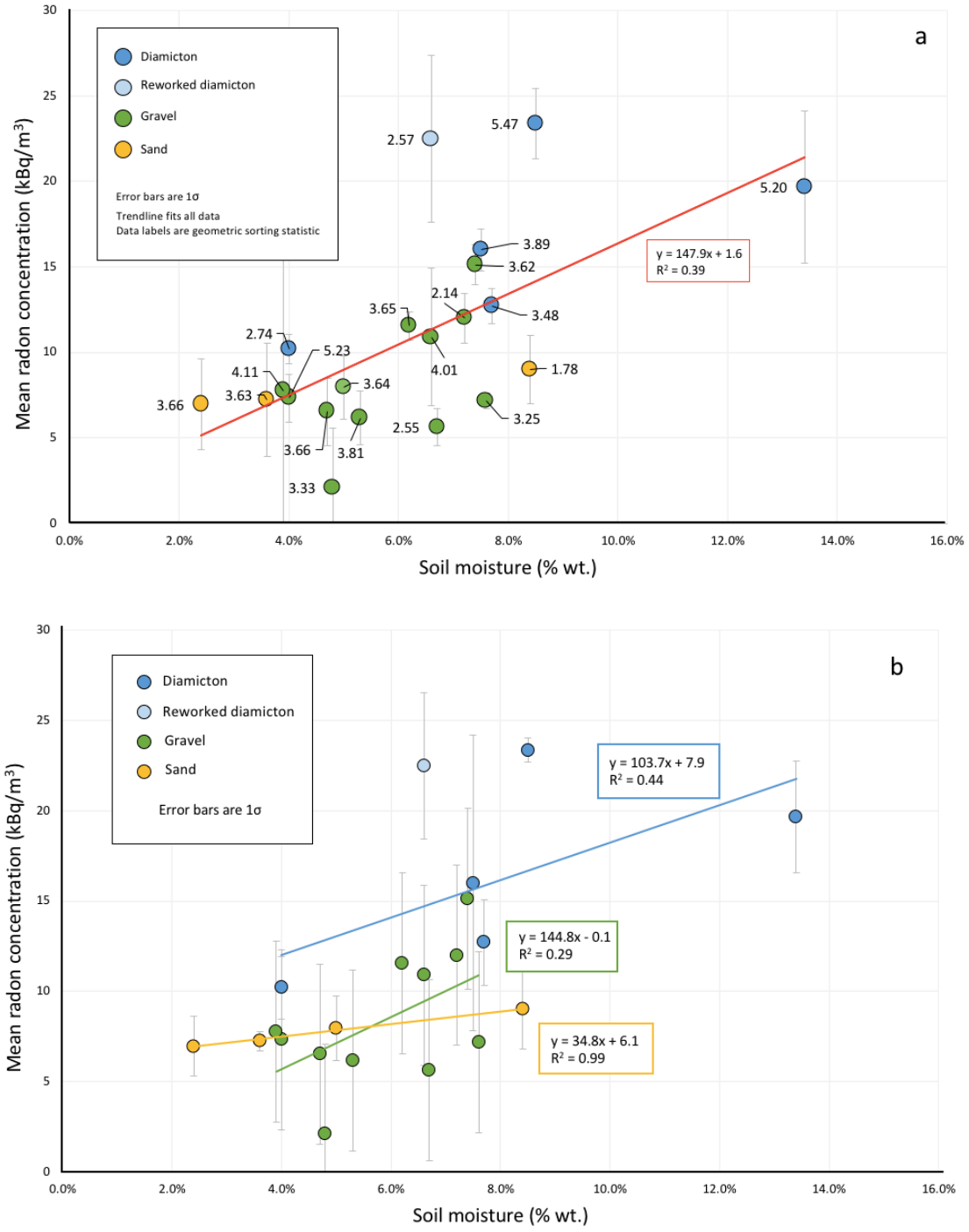

Figure 16 – Mean radon concentration compared to moisture at 60 cm depth. Trendlines calculated for (a) all samples and (b) each major sediment type. Data labels correspond to geometric sorting statistic of the matrix. Moisture is calculated as fraction of water by mass and was measured by mass difference of sediment from soil pit before and after heat treatment. All means were calculated only from measurements on the day a soil pit was dug (five measurements instead of ten).

4.8 Sediment geochemistry

4.8.1 Matrix

The results of the geochemical analysis for major, selected minor, and trace elements are provided in Appendix 3. To determine whether the concentration of ^{238}U in nearby sediment is a significant control on radon concentration at 60 cm depth, I compared uranium concentration in a matrix sample collected from the soil pit to CoV-weighted radon concentration at the corresponding site. I observed no correlation between uranium content of matrix and radon concentration (Fig. 17) in either the entire sample population or in individual sediment types. For example, diamicton sites typically displayed relatively high ^{222}Rn concentration, but the corresponding matrix samples did not display the highest concentrations of uranium. The clustering of diamicton suggests relatively uniform composition across the study area, however the number of samples is insufficient to confirm this.

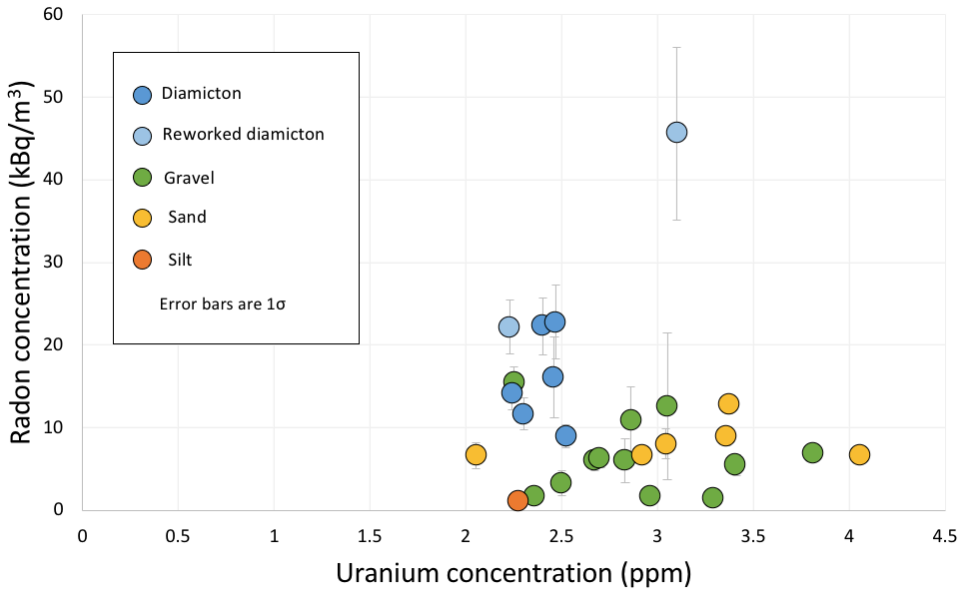

Figure 17 – Mean radon concentration compared to uranium content of matrix. Data points coloured according to textural classification of sediment.

Recognizing that U^{2+} tends to substitute for Ca^{2+} in minerals, a sediment composed of few calcium-bearing minerals may lack substitution sites for uranium, and may thus have lower radon activity. While this does not affect the uranium-radon relationship (Fig. 17), sediment mineralogy could cause significant variation in the uranium concentration of different sediment

types as suggested by my examination of maturity. Although not a complete test for this relationship (since U can occur in other situations than calcium-substitution), I normalized the uranium concentration with respect to calcium concentration and compared to radon (Fig. 18). No correlation was observed between calcium-normalized uranium concentration in the sediment matrix and measured soil radon concentration.

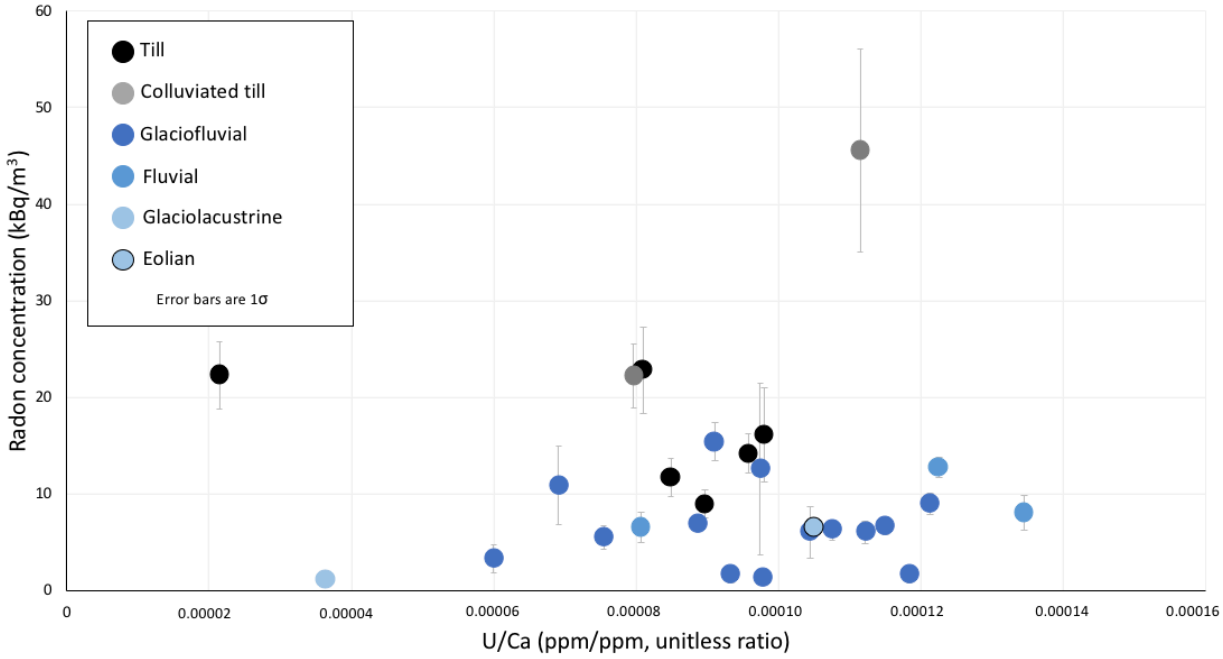

Figure 18 – Mean radon concentration compared to uranium concentration of matrix (normalized to calcium concentration).

To determine whether uranium-bearing minerals such as apatite and zircon were significant sources of uranium in the sediment matrix samples, uranium concentration was compared to phosphorus (as a proxy for apatite) and zirconium (as a proxy for zircon). I observed weak positive correlation in both cases, suggesting these minerals are at least partial sources of uranium and therefore radon in the Whitehorse sediments (Fig. 19). More analyses are needed to confirm this, including optical microscopic analysis of grain mounts of the sediments on more representative samples than I collected.

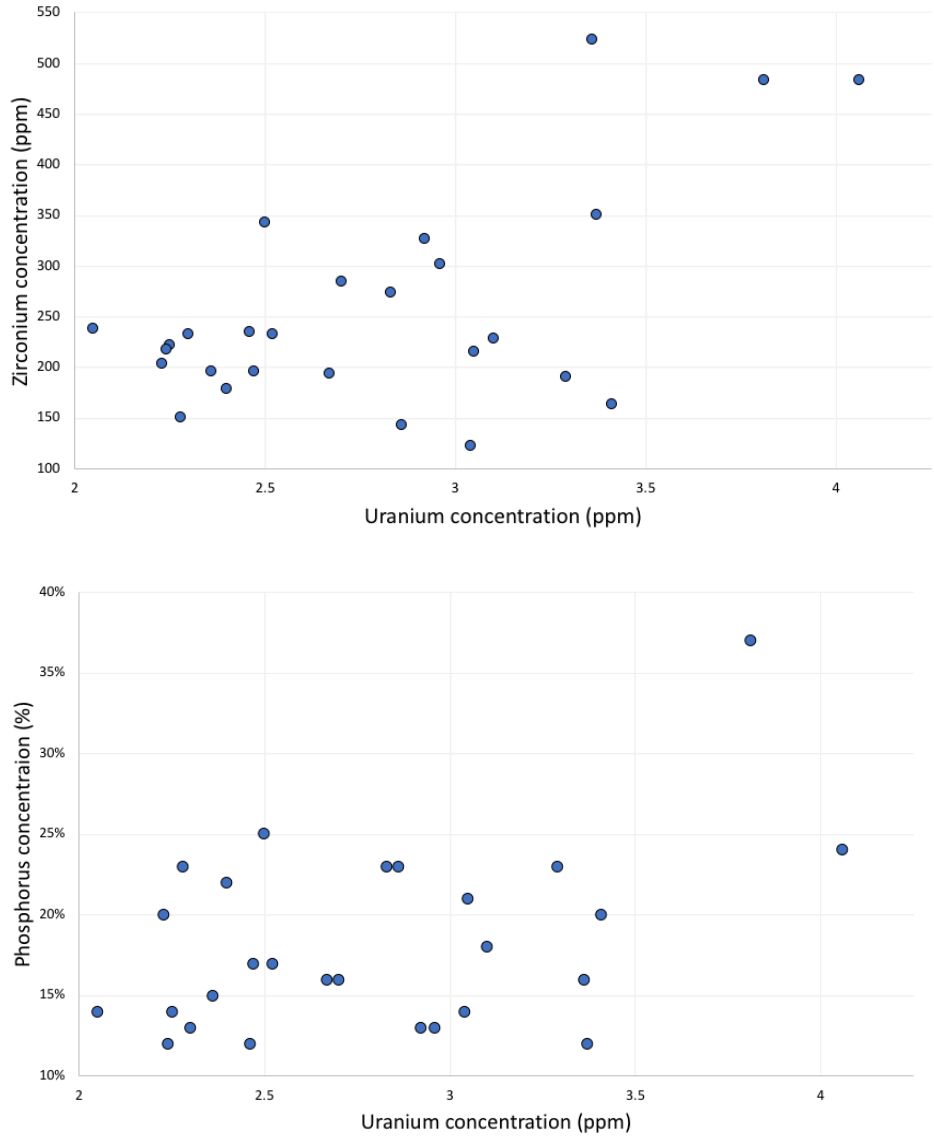

Figure 19 – Comparisons of phosphorus and zirconium concentrations with uranium concentration in sediment matrix. These elements serve as proxies for the uranium-bearing minerals apatite and zircon, respectively. Error bars not included due to high precision of lab data.

In summary, four geochemical indices – uranium, uranium normalized with respect to calcium, zirconium (as proxy for zircon), and phosphorus (as proxy for apatite) – all suggest that uranium in nearby sediment is not a significant control on radon concentration at 60 cm depth.

4.8.2 Clasts

I also conducted geochemical analyses on representative clasts from the sampled soil pits to determine if uranium concentration in clasts is a controlling factor on radon gas concentration at 60 cm depth. Clasts may be important contributors of subsurface radon in sediments where they are abundant (e.g. certain gravel sites) and when they are composed of resistant rock types whose composition is not reflected in the matrix. These clasts typically ranged in size from 5-10 cm, and were classified as granite, basalt, limestone, clastic sedimentary, fine-grained crystalline (volcanic), and fine-grained crystalline containing phenocrysts (porphyries). The uranium concentration of these representative clasts was then compared to radon concentration at the corresponding site. Since I analyzed only representative clasts from selected soil pits, and not every clast from each site, this comparison is rather crude. I did not analyze all clasts from a single pit either, so a calculation of equivalent uranium at a single site was not possible. Instead, I classified and counted 50-100 clasts from each site according to the above lithologies to determine the relative abundance of major clast lithologies, and analyzed select representative clasts geochemically, whose abundance and uranium concentration are compared to radon concentration in Figure 20. Note that not all sites are represented as some soil pits did not have clasts, and that in certain cases multiple lithologies from a single soil pit were chosen for analysis.

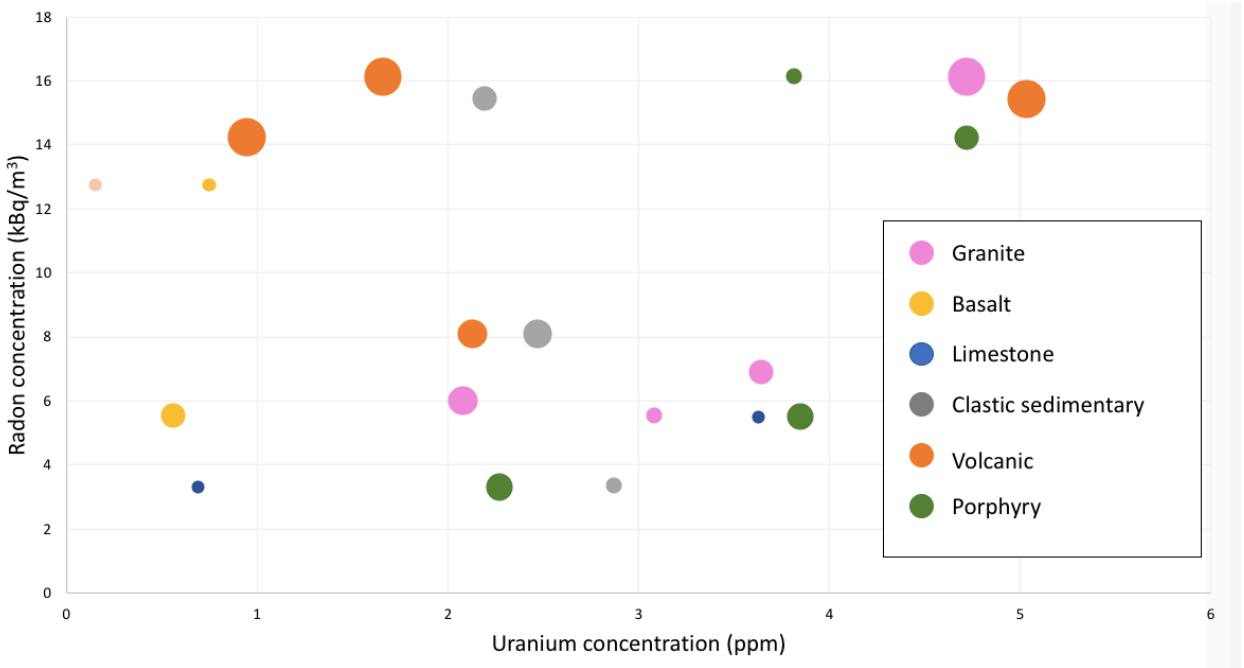

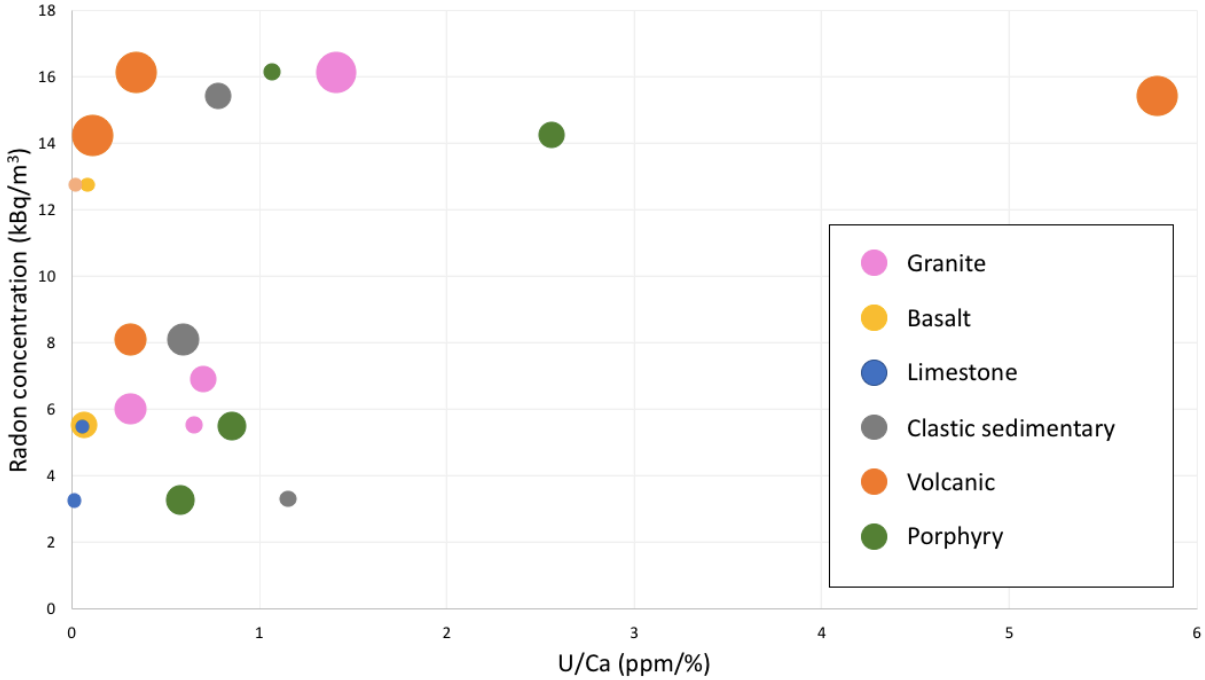

Figure 20 – Uranium concentration of representative clast lithologies compared to radon concentration. Uranium normalized with respect to calcium in order to confirm the presence of uranium-bearing minerals (via calcium substitution). Data point colours correspond to lithology and size corresponds to relative abundance of lithology type based on pebble count. Largest circles represent roughly 40% abundance, smallest circles represent <5% abundance.

Uranium concentration, both unmodified and normalized to calcium concentration, appears to lowest in basalt and limestone clasts. This may reflect the incompatibility of uranium in mantle-derived basalts, the low abundance of uranium in marine water, and the relatively high calcium content of these rock types (yielding a low U/Ca ratio in the normalized graph). Felsic lithologies (volcanic, porphyry, and granite) all have relatively higher uranium and uranium/calcium ratios, while neither uranium nor uranium/calcium varies significantly in clastic sedimentary clasts.

A weak correlation between uranium concentration in the felsic clasts and radon concentration in sediment is possible, but I have insufficient data to test this statistically. Increased uranium concentration in a clast may be related to higher radon concentration at the corresponding site, but there are clearly other, stronger controlling factors on radon concentration at this depth.

4.9 Statistical analysis

While there is insufficient data in the Yukon soil radon dataset at this time, I conducted two preliminary statistical tests on the available data to help guide future work and hypotheses to test. The results of these tests could recommend changes in soil radon sampling protocols (such as waiting a day after significant rainfall before sampling). The two tests I conducted were univariate correlation and multivariate principal component analysis. I used these tests to determine which (if any) of the suspected controls on radon concentration in surficial sediment may explain the variances observed in the previously described results. Specifically, I compared the effects of matrix uranium concentration, silt and clay content of matrix, soil moisture, geometric sorting statistic, and depth to bedrock, on measured radon concentration.

In univariate correlation, the Pearson correlation coefficient (r) is calculated between each pair of variables. These are reported in graphical format using PAST4 software (Hammer *et al*., 2001) (Fig. 21). Only the top row, that is, the correlation of each variable with mean radon concentration, is of interest to this study. The strongest positive correlation is between radon and silt/clay content of matrix, corroborating the results in §4.4 on grain size distribution (Fig. 12). A relatively strong positive correlation also exists with soil moisture, consistent with §4.7 results (Fig. 16), and a weak positive correlation with sorting statistic (§4.5; Fig. 13). I also observe weak negative correlations between radon and depth to bedrock, and uranium content of matrix.

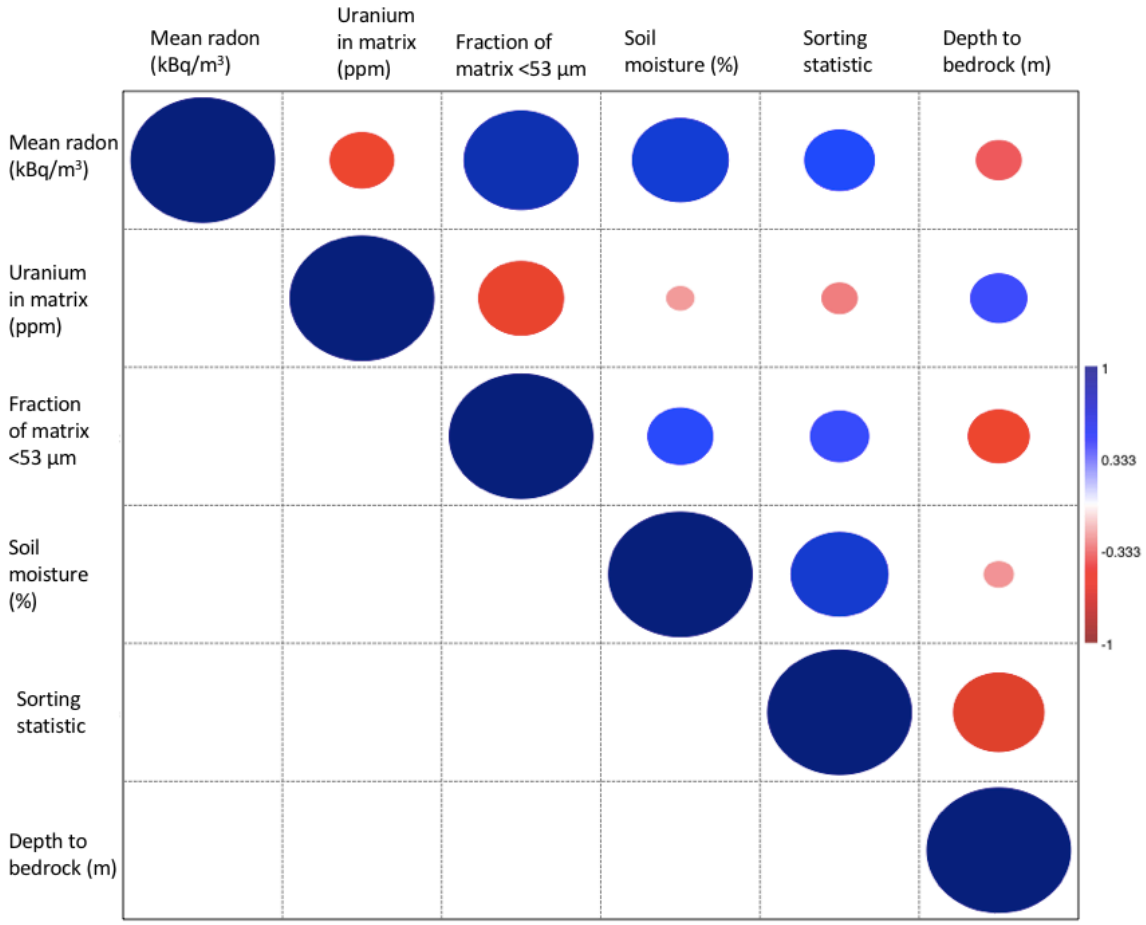

Figure 21 – Univariate correlation of suspected controls on radon concentration. Blue indicates positive correlation while red indicates negative correlation. Size of circle indicates magnitude of correlation, where the large blue circles indicate perfect 1:1 correspondence. Figure produced by PAST4 software package (Hammer *et al*. 2001).

In principal component analysis, data points are plotted as vectors in which each variable (in this case controls on radon such as matrix fine fraction, sorting statistic, and depth to bedrock) corresponds to a unique dimension The analysis consists of determining the eigenvectors of the resultant matrix. Consequently, closely aligned variables are more closely correlated, while orthogonal vectors are unrelated. Although the dataset collected this summer is not ideal for principal component analysis (lacking sufficient data points and variables for effective analysis), PCA nonetheless reveals several interesting trends (Fig. 22).

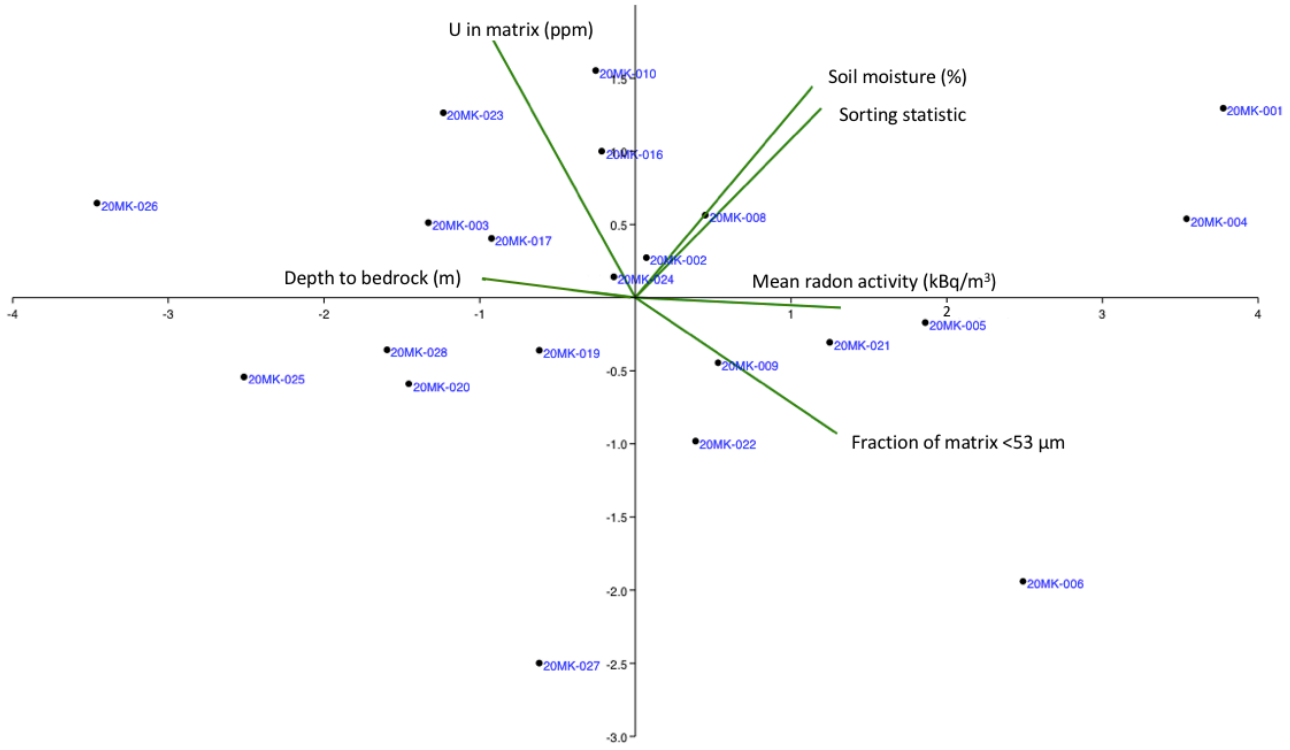

Figure 22 – Principal component analysis of suspected controls on radon concentration. Black dots are data points, green lines are compared variables. Alignment of lines indicates correlation; orthogonal lines are unrelated. Figure produced by PAST software package (Hammer *et al.* 2001).

For one, radon concentration in sediment and uranium concentration of matrix are nearly orthogonal, indicating little to no dependence, corroborating the geochemistry results. This suggests that uranium in sediment matrix is not a significant source of radon in near-surface settings. The strongest correlation is between sediment moisture and sorting, which are almost completely aligned. Overall, the statistical analyses, although limited in confidence owing to insufficient data, support the interpretations that (i) sediment moisture may be a function of sorting, and (ii) soil moisture, silt and clay content of matrix, and sorting are all somewhat related to radon concentration in sediment.

5. Discussion and implications

I successfully tested the hypothesis that the grain size distribution of surficial sediments is a strong control on near-surface radon concentration, corroborating laboratory and modelling studies (e.g. Thu *et al*., 2020; Sakoda *et al*., 2010). By examining a wide variety of possible controls, including bedrock type, physical characteristics of sediment, and sediment geochemistry, I determined that the silt and clay content of a sediment is indeed a strong control on radon concentration. I also noted several other, possibly related, controls on radon concentration. One is sediment moisture, which correlates positively with radon concentration and may be related to sediment permeability and water-holding capacity of the clays it contains. Another strong control is sediment maturity, which displays negative correlation with radon concentration. Fine-grained glaciolacustrine sediments display low radon concentration, suggesting that silt and clay content is not the only strong control on radon in sediment, and that the reworking of material may also affect radon concentration significantly. By combining the data from my summer field work with monthly data collected by the Yukon Geological Survey in fall of 2019, I noted a strong seasonal variation in radon concentration. I have accomplished my objectives of constraining numerous geological and meteorological parameters to determine first-order controls on radon concentration.

Seasonality appears to be an important non-geologic control on soil radon concentration in the region of Whitehorse, Yukon. While relatively consistent from May to August and from December to January, measured concentrations from 2019 and 2020 differ significantly between the two periods. Seasonal variability has been widely observed in outdoor and indoor studies (e.g., Siino *et al*., 2019; Yang *et al*., 2017; Barazza *et al*., 2015). However, not all sediment types in the Whitehorse region display consistent variation, as two sediment types exhibit higher and one sediment type lower radon concentrations in the summer (Fig. 10). A particular consideration for seasonal variation in Whitehorse is the seasonal freezing and thawing of ground, possibly creating a frozen cap which traps radon below the surface (Fig. 23). Due to lower permeability in the silt-rich till (20MK-15), the retention of soil moisture as ice in the winter months may have reduced soil radon flux in the till more substantially.

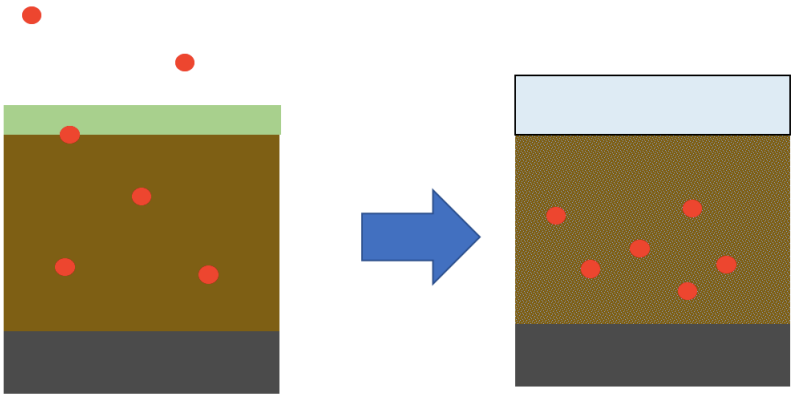

Figure 23 – Frost cap diagram. Red dots represent gaseous radon atoms, which are transported to through unfrozen sediment to the surface during the summer (left) where they dissipates, compared to winter (right), when frozen sediment and snow at the surface trap radon belowground, possibly concentrating radon below the surface in the winter.

The apparently opposite trends of seasonal variation of radon concentration in different sediments motivated an analysis of the potential causes of non-seasonal variability in Yukon soil radon flux. Of the parameters evaluated—bedrock lithology, thickness of surficial cover, surficial sediment type, grain size distribution, sorting, sediment maturity, soil moisture, and matrix and clast geochemistry—silt and clay content of the matrix and sediment maturity appear to be the strongest controls on soil radon concentration in sediment.

A grain-size control in the study area is most evident from the positive correlation of radon concentration and quantity of silt and clay in the surficial sediment (Fig. 12). The observed seasonal anti-phasing seems to correspond with local differences in texture, where sites 20MK-013 and 20MK-014 have dominantly sandy matrices and overall textures of sand or gravelly muddy sand, whereas site 20MK-015 is a glacial diamicton with a greater silt component and therefore relatively lower permeability.

Grain size has previously been attributed as a first order control on soil radon flux (Thu *et al.*, 2020; Sakoda *et al.*, 2010; Markannen and Arvela, 1992). However, fine-grained glaciolacustrine sediments examined in this study do not display high concentrations of radon. This suggests that sediment maturity may also control radon concentration. For example, tills, which are relatively recently derived from bedrock and have sandy silt matrices, tend to contain high levels of radon compared to similarly fine-grained glaciolacustrine sediments. It is possible that as the glaciolacustrine sands and silts are reworked, the uranium-bearing minerals are

weathered and destroyed. Overall, radon concentration tends to decrease with sediment maturity (Fig. 14).

A positive correlation is observed between radon concentration and soil moisture (Fig. 16), and this may reflect both average grain size and porosity of these sediments. While water may facilitate the transport of radon by dissolution, it seems likely that in this case it is inhibiting gas flux. This is supported by laboratory and modelling studies by Thu *et al*. (2020) and others, which suggest that water impedes the diffusion of radon by blocking pore spaces. This effect is enhanced in samples with small grains, since the pore spaces are also smaller. In near surface settings, water may prevent the diffusion of radon, thereby enhancing its concentration below ground.

Depth to bedrock does not appear to be a first-order control on radon concentration, at least in areas where surficial material thickness is greater than 1 m. A site in 1.5 m of sediment of overlying granodiorite displays concentrations of radon much lower than in the proximate bedrock derivative, suggesting that sediment greatly reduces the flux of radon. This site was sampled incompletely at the end of the field season, and thus is not included in many of the comparisons of radon with environmental characteristics. Anecdotally, it seems to suggest the sediment is a strong moderator of radon flux. In general, it seems that diffusion and emanation from bedrock minerals is not the sole source of radon nor is it a first-order control of spatial and temporal variability. Previous studies (e.g., O'Brien *et al.*, 2011) seem to support this observation, where bedrock-to-surface transport time exceeded the lifetime of ^{222}Rn. Variable chemical composition of the different Quaternary sediment types overlying a single bedrock type could help further explain the source of variation in radon concentration.

In addition to my own and previous observations of the relationship between grain size and radon concentration, it may be worthwhile to explore the escape of ^{222}Rn from uranium-bearing minerals. Emanation of ^{222}Rn is controlled by its recoil distance from the alpha decay of ^{226}Ra, which must therefore be within tens of micrometres of the grain surface for ejection to occur (Nazaroff, 1992). Therefore, sediments with finer grain sizes and higher surface area-to-volume ratio may have a larger contribution to soil gas radon (Sakoda *et al*., 2010) , particularly if the fine fraction is a close derivative of bedrock. Furthermore, the fate of the ^{222}Rn after it escapes the grain may also be controlled by grain size, permeability, sorting, and moisture

content. Sakoda *et al.* (2010) have considered some of these possible controls through numerical modeling, and their approach merits further analysis based on the available data from this study.

Although previous work (e.g. Kishchuk *et al*., 2021) suggests that factors such as grain size distribution and maturity may control the production of radon in sediment, geochemical analysis indicates that neither matrix nor clasts at 60 cm depth are a principal source of radon. Uranium concentration in either sediment component sampled from the soil is not clearly correlated to radon concentration at the corresponding site, suggesting that the controls examined in this study are primarily controls on radon sinks. This is corroborated by the seasonal variability of the readings, which suggests that regardless of constant radioactive decay and thus radon production, there is significant variation in near-surface concentration. Intuitively, it seems likely that much of the radon exhaled at the surface is produced at depths greater than 60 cm and then transported to sampling depth. I therefore conclude that the factors examined in this study are mostly controls on transport, not production.

Almost all of the measured soil radon concentrations were above the Canadian recommended limit for indoor radon exposure of 0.2 kBq m^{-3}. An analysis of the link between soil radon concentration and indoor radon concentration is highly recommended in order to assess how surficial geology and dwelling architecture contribute to risks of radon exposure in Yukon. Many basements in the Whitehorse area are founded in sediment, not bedrock.

In summary, my analysis of the 2020 soil radon data indicates that bedrock is neither the single nor the most important source or control of near-surface soil radon concentration in the Whitehorse area. Of the surficial sediment parameters measured, silt and clay content of the soil matrix is the most closely correlated to radon concentration. Sediment maturity also appears to be a strong control on radon concentration. Several meteorological factors, such as moisture and season, impart appreciable temporal variability on soil radon concentration among different sediment types. Future field programs targeting the source of variability should include more long-term continuous sampling at selected sites to evaluate the strength and reproducibility of the apparent seasonality, and additional sites in eolian and glaciolacustrine units are needed for a more representative characterization of the regional soil radon flux. I also recommend an overall increase in the number of sample sites to strengthen the statistics, and continuous measurement of at least some of the sites examined in this study to provide the long-term monitoring necessary to address temporal changes in soil radon flux.

6. Conclusions

Radon concentration was measured in sediment at 30 sites throughout the Whitehorse area. These sites represent till, glaciofluvial sand and gravel, fluvial sand and gravel, glaciolacustrine silt, and eolian sand. They overlie granodiorite, limestone, clastic sedimentary and basalt bedrock in various combinations. Almost all sites are in undisturbed sediment. A variety of geological controls (bedrock and sediment type, surficial cover thickness, grain size distribution, sorting, sediment maturity, soil moisture) and meteorological factors (rainfall, air pressure, wind, temperature) were compared to soil radon concentration.

A notable seasonal shift in soil gas radon concentrations was observed at three long-term monitoring sites representing fluvial sand, glaciofluvial gravel and lodgement till. In the gravel site, radon concentration was at its lowest from May to August, while concentration in the diamict site was highest during these months. Relative to the seasonal variation, soil radon concentration was consistent during the summer months when most of this study was undertaken, and so intraseasonal variability likely had little effect on the results reported here.

Radon concentration is found to be independent of depth to bedrock, and shows no clear correlation with bedrock type. Grain size distribution and sediment maturity appear to be the strongest geological controls on radon concentration in the surficial cover. It also appears that soil radon concentration correlates positively with soil moisture and negatively with sediment maturity. Geochemical analysis reveals a lack of correlation between uranium content of matrix and clasts at 60 cm depth, suggesting that the controls investigated in this study are primarily controls on transport.

The natural occurrence of this carcinogenic gas appears to be contingent on a wide range of factors, including but not limited to: season, sediment grain size distribution, sediment maturity, and moisture. While not dangerous in outdoor settings, many Whitehorse homes are founded in sediment with highly variable and possibly hazardous radon concentrations. Further work is therefore recommended to correlate geologic controls on radon concentration with anthropogenic controls in the built environment.

References

Barazza, F., Gfeller, W., Palacios, M. and Murith, C., 2015. An investigation of the potential causes for the seasonal and annual variations in indoor radon concentrations. Radiation Protection Dosimetry, vol. 167, p. 75–81.

Blott, S.J. and Pye, K., 2001. GRADISTAT: a grain size distribution and statistics package for the analysis of unconsolidated sediments. Earth Surface Processes and Landforms, vol. 26, p. 1237–1248.

Bond, J.D., 2004. Late Wisconsinan McConnell glaciation of the Whitehorse map area (105D), Yukon. *In:* Yukon Exploration and Geology 2003, D.S. Emond and L.L. Lewis (eds.), Yukon Geological Survey, p. 73–88.

Bond, J., Morison, S. and McKenna, K., 2005a. Surficial Geology of MacRae (NTS 105D/10), Yukon (1:50 000 scale). Yukon Geological Survey, Geoscience Map 2005-6.

Bond, J., Morison, S. and McKenna, K., 2005b. Surficial Geology of Whitehorse (NTS 105D/11), Yukon (1:50 000 scale). Yukon Geological Survey, Geoscience Map 2005-7.

Bond, J., Morison, S. and McKenna, K., 2005c. Surficial Geology of Upper Laberge (NTS 105D/14), Yukon (1:50 000 scale). Yukon Geological Survey, Geoscience Map 2005-8.

Brideau, M.-A., Stead, D., Bond, J.D, Lipovsky, P.S. and Ward, B.C., 2011. Preliminary stratigraphic and geotechnical investigations of the glaciolacustrine and loess deposits around the city of Whitehorse (NTS 105D/11), Yukon. *In*: Yukon Exploration and Geology 2010, K.E. MacFarlane, L.H. Weston, and C. Relf (eds.), Yukon Geological Survey, p. 33–53.

Cinelli, G., Tositti, L., Capaccioni, B., Brattich, E., and Mostacci, D., 2015. Soil gas radon assessment and development of a radon risk map in Bolsena, Central Italy. Environmental Geochemistry and Health, vol. 37, p. 305–319.

Colpron, M. (comp.), 2011. Geological compilation of Whitehorse trough - Whitehorse (105D), Lake Laberge (105E), and part of Carmacks (115I), Glenlyon (105L), Aishihik Lake (115H),

Quiet Lake (105F) and Teslin (105C). Yukon Geological Survey, Geoscience Map 2011-1, 3 maps, scale 1:250 000, legend and appendices.

Folk, R. L. and Ward, W. C., 1957. Brazos River bar: a study in the significance of grain size parameters. Journal of Sedimentary Petrology, vol. 27, p. 3-26.

Friske, P.W.B., Kettles, I.M., McCurdy, M.W., McNeil, R.J., and Harvey, B.A., 2010. North American Soil Geochemical Landscapes Project: Canadian field protocols for collecting mineral soils and measuring soil gas radon and natural radioactivity. Geological Survey of Canada, Open File 6282, 177 p.

Government of Canada, 2020. Radon – What you need to know. Health Canada, <https://www.canada.ca/en/health-canada/services/environmental-workplace-health/reports-publications/radon-what-you-need-to-know.html > [accessed December 10, 2020].

Government of Yukon, 2020. Radon information map, < https://yukon.maps.arcgis.com/apps/MapSeries/index.html?appid=b0b4f261617541e8b715e7aafc79c846 >, [accessed November 30, 2020].

Government of Yukon, 2018. Radon testing in Yukon schools <https://yukon.ca/en/learn-about-radon-testing-yukon-schools#radon-testing-in-yukon-schools>, [accessed November 30, 2020].

Hammer, Ø., Harper, D.A.T., and P. D. Ryan, 2001. PAST: Paleontological Statistics Software Package for Education and Data Analysis. Palaeontologia Electronica, vol. 4, 9pp.

Hart, C.J.R. and Radloff, J.K., 1990. Geology of Whitehorse, Alligator Lake, Fenwick Creek Carcross and Part of Robinson Map Areas (105D/11, 6, 3, 2 & 7). Yukon Geological Survey, Open File 1990-4(G).

Kishchuk, M.J., Lipovsky, P.S., Bond, J.D. and Gosse, J.C., 2021. Preliminary investigation of geological controls on radon concentration in surficial sediment in Whitehorse, Yukon (NTS 105D/11, 14). In: Yukon Exploration and Geology 2020, K.E. MacFarlane (ed.), Yukon Geological Survey, p. 115-135.

Marin, P.C., 1956. Measurement of the half-life of radon with a Curie-type ionization chamber. British Journal of Applied Physics, vol. 7, p. 188–190.

Markannen, M. and Arvela, H, 1992. Radon emanation from soils. Radiation Protection Dosimetry, vol. 45, p. 269–272.

Nesbitt, H.W. and Young, G.M., 1982. Early Proterozoic climates and plate motions inferred from major element chemistry of lutites. Nature, vol. 299, p. 715-717.

Nazaroff, W. M., 1992. Radon transport from soil to air. Review of Geophysics, vol. 30, p. 137-160.

O'Brien, K.E., Goodwin, T.A. and Risk, D., 2011. Radon soil gas in the Halifax Regional Municipality, Nova Scotia, Canada. Atlantic Geology, vol. 47, p. 112–124.

Pearson, F.K., Hart, C.J.R. and Power, M., 2001. Distribution of Miles Canyon basalt in the Whitehorse area and implications for groundwater resources. *In:* Yukon Exploration and Geology 2000, D.S. Emond and L.H. Weston (eds.), Exploration and Geological Sciences Division, Yukon Region, Indian and Northern Affairs Canada, p. 235–245.

Porstendorfer, J., 1994. Properties and behavior of radon and thoron and their decay products in the air. Journal of Aerosol Science, vol. 25, p. 219–263.

Sakoda, A., Ishimori, Y., Hanamoto, K., Kataoka, T., Kawabe, A. and Tamaoka, K., 2010. Experimental and modeling studies of grain size and moisture content effects on radon emanation. Radiation Measurements, vol. 45, p. 204–210.

Siino, M., Scudero, S., Cannelli, V., Piersanti, A. and D'Alessandro, A., 2019. Multiple seasonality in soil radon time series. Scientific Reports, vol. 9, 13 p.

Stanley, F. K. T., Irvine, J.L., Jacques, W.R., Salgia, S.R., Innes, D.G., Winquist, B.D., Torr, D., Brenner, D.R. and Goodarzi, A.A., 2019. Radon exposure is rising steadily within the modern North American residential environment, and is increasingly uniform across seasons. Scientific Reports, vol. 9, 17 p.

Thu, H. N. P., Thang, N. V. and Hao, L. C., 2020. The effects of some soil characteristics on radon emanation and diffusion. Journal of Environmental Radioactivity, vol. 216, 13 p.

Wentworth, C. K., 1922. A Scale of Grade and Class Terms for Clastic Sediments. The Journal of Geology, vol. 30, p. 377-392.

Wolfe, S., Bond, J. and Lamothe, M., 2011. Dune stabilization in central and southern Yukon in relation to early Holocene environmental change, northwestern North America. Quaternary Science Reviews, vol. 30, p. 324–334.

World Health Organization, 2009. WHO handbook on indoor radon: a public health perspective. WHO Press, Geneva, 94 p.

Yang, J., Buchsteiner, M., Salvamoser, J., Irlinger, J., Guo, Q. and Tschiersch, J., 2017. Radon exhalation from soil and its dependence on environmental parameters. Radiation Protection Dosimetry, vol. 177, p. 21–25.

Yukon Geological Survey, 2020a. Yukon digital bedrock geology. Yukon Geological Survey, http://data.geology.gov.yk.ca/Compilation/3#InfoTab, [accessed November 30, 2020].

Yukon Geological Survey, 2020b. Yukon Lithogeochemistry data set. Yukon Geological Survey, http://data.geology.gov.yk.ca/Compilation/35#InfoTab, [accessed December 1, 2020].

Yukon Housing Corporation, 2018. Whitehorse Indoor Radon Test Results 2006-2018. Yukon Housing Corporation, https://yukon.ca/en/radon, [accessed November 26, 2020].

Yukon MINFILE, 2021. Yukon MINFILE – A database of mineral occurrences. Yukon Geological Survey, <http://data.geology.gov.yk.ca/Occurrences> [accessed March 7, 2021].

Appendix 1 – Sample site characteristics

Site	Bedrock Type	Depth to Bedrock (m)	Soil profile	Vegetation/drainage	Elevation (m)	Latitude/Longitude	Disturbance
20MK-001	Limestone	29	0-14 cm: Organics 14-50 cm: Matrix supported ablation till Sandy silt matrix 50-65+ cm: Basal till, silt and clay matrix	Mature white spruce forest Feather moss and soapberry groundcover. Poorly drained.	770	60.7389N/135.1422W	No White River Ash (WRA).
20MK-002	Limestone	5.5	0-10 cm: Organics 10-30 cm: Loess with charcoal lenses Silt with minor sand 30-60 cm: Glaciofluvial gravel Silty coarse sand matrix supported. 70% pebbles, 30% cobbles	White spruce, young aspen, willow forest. Feather moss, cranberry, rosehip groundcover. Moderately well-drained.	759	60.7384N/135.1422W	No WRA Sparse root-thrown pebbles to 30 cm.
20MK-003	Limestone	10	0-5 cm: Organics 5-12 cm: Loess 12-60 cm: Clast-dominated gravel. 70% pebbles, 30% cobbles.	Mixed aspen, willow, and spruce forest. Soapberry, rosehip, and kinnikinnick groundcover. Well-drained.	777	60.7375N/135.1433W	No WRA, tree-thrown cobbles to 12cm. Fine roots to 45cm.
20MK-004	Limestone	8.5	0-5 cm: Organics 5-11 cm: Oxidized loess Gradational contact with till	Pine and willow forest. Kinnikinnick, feather moss, lupine, soapberry groundcover. Moderately well-drained.	764	60.7392N/135.1414W	Discontinuous WRA. Fine roots to 40cm.
20MK-005	Granodiorite	1.5	0-6 cm: Organics 6-10 cm: Tephra Somewhat discontinuous 8-32 cm: Loess Oxidized to 14 cm, very fine-grained sand 32-60+ cm: Basal till 40% clasts, 60% matrix Clasts are 60% cobbles, 40% pebbles	Open spruce and willow forest. Patchy kinnikinnick. Moderately well-drained.	788	60.7379N/135.1386W	WRA present but not continuous. Evidence of human disturbance such as old trenches and vehicles ruts. Site positioned on undisturbed groundcover.
20MK-006	Granodiorite	?	0-6 cm: Organics 6-60+ cm: Fine-grained sand and silt No bedding or clasts observed	Spruce forest, feather moss groundcover. Alder and willow line trail.	746	60.7429N/135.1356W	Discontinuous WRA. Site straddles an ATV trail. Roots to 50cm.
20MK-007	Granite	9	0-9 cm: Organics 9-20 cm: Dark brown sandy soil Charcoal layer at 10 cm 20-60+ cm: Silt Very fine-grained, no bedding or clasts Frozen below 45 cm	Mature pine forest, willows growing over road. Ground is carpeted with thick feather moss. Poorly-drained.	828	60.6211N/135.0485W	No evidence of WRA. Site is on an overgrown exploration road (surficial dirt track, not cut into ground). Roots to 14 cm.
20MK-008	Granite/skarn	2	0-6 cm: Organics 6-40 cm: Loess Uneven gradational contact between oxidized and fresh layers 33+ cm: Gravel 65% sandy matrix, 35% clasts 10% small boulders, 40% cobbles, 50% pebbles Irregular contact with overlying loess	Mature spruce hung with lichen. Ground carpeted with thick feather moss. Bedrock outcrops. Poorly drained.	841	60.6207N/135.0417W	Discontinuous WRA.
20MK-009	Limestone	?	0-6 cm: Organics 6-12 cm: Loess 12-60+ cm: Gravel 50% clasts (subrounded), 50% matrix (sand with minor silt) 30% pebbles, 60% cobbles, 10% small boulders	Mixed spruce and pine forest with some mature willows. Groundcover: reindeer lichen, kinnikinnick, lupine, soapberry. Well drained.	842	60.6233N/135.0455W	WRA mixed with loess layer. No human disturbance.
20MK-010	Seds	17	0-4 cm: Organics 4-25 cm: Oxidized sand 20-60+ cm: Gravel 55% matrix (medium to coarse grained sand) 45% clasts (40% small boulders, 35% cobbles, 25% pebbles)	Mature spruce forest, with willow and sparse pine. Groundcover dominated by feather moss, reindeer lichen, and kinnikinnick. Well drained.	848	60.6225N/135.0487W	Patchy WRA. Roots to 40 cm.
				Mixed spruce and aspen with minor pine and birch.			No WRA.

				Groundcover dominated by kinnikinnick, feather moss, and Labrador tea.			Site located on edge of quarry pit, soil not locally disturbed.
20MK-011	Limestone	<1	Veneer till overlain by organics	Well drained.	758	60.7387N/135.1437W	
				Spruce forest. Reindeer lichen and kinnikinnick groundcover.			
20MK-012	Granodiorite	1.5	Loess and sandy gravell overlying granitic grus bench	Well drained.	764	60.7366N/135.1480W	No WRA observed, no human disturbance.
			0-3 cm: Organics 3-60 cm: Medium- to fine-grained sand	Open pine forest with a few spruce and aspen. Groundcover is rosehips, grass, and soapberry.			No WRA observed.
20MK-013	Granodiorite	>16		Well drained.	699	60.7379N/135.0985W	Dug pits and piles of dirt, no probes are in these old pits.
			0-10 cm: Organics 10-25 cm: Medium- to coarse- grained sand with silt interspersed 25-60 cm: Gravel Rounded to sub-rounded clasts in sandy matrix. 25% matrix, 75% clasts. 30% small boulders, 60% cobbles,	Aspen forest, with some mature willow and spruce. Groundcover is soapberry, grass, kinnikinnick. Well drained.			No WRA observed. Fine roots to 40 cm.
20MK-014	Granodiorite	91.5	10% pebbles.		734	60.6784N/135.0519W	
			0-10 cm: Organics and tephra 10-35 cm: Loess, oxidized to 20 cm 35-60+ cm: Till 70% silty sand matrix, 30% clasts.	Spruce forest with some pine. Groundcover is feather moss, cranberry, soapberry, lupine. Poorly drained.			
20MK-015	Granodiorite	>76	25% cobbles, 75% pebbles.		757	60.6751N/135.0552W	Continuous WRA.
			0-6 cm: Organics and tephra 6-16 cm: Loess, gradational contact with underlying unit 16-42 cm: Medium- to coarse-grained sand with negligible silt 42-60+ cm: Gravel Subrounded to rounded clasts in sandy matrix. 60% matrix, 40% clasts. Matrix is medium- to coarse-grained sand. Clasts are 10% small boulders,	Mixed pine, spruce, and aspen forest. Some willow saplings. Groundcover is large mats of feather moss with crowberry, soapberry, lupine, and kinnikinnick. Well drained.			Discontinuous WRA. Root-thrown cobbles in sand layer.
20MK-016	Basalt	32	25% cobbles, and 65% pebbles.		661	60.6970N/135.0246W	
			0-5 cm: Organics 5-12 cm: Loess Patchy, mixed with underlying layer 5+ cm: Medium-grained sand, no bedding observed, sparse pebbles and	Mixed spruce and pine forest Soapberry, kinnikinnick, and feather moss groundcover.			
20MK-017	Granodiorite	>93	cobbles	Well-drained.	642	60.7019N/135.0127W	No WRA (fluvial deposit, so does not signal disturbance).
				Spruce forest with aspen trees (depending on aspect).			No WRA (Clay Cliffs)
20MK-018 (Lowe	Granodiorite	77	Glaciolacustrine silt deposit. Bedding evident in outcrops	Very poorly drained.	669	60.7151N/135.0585W	Undisturbed in sample location.
			Upper section of 20MK-018 silt deposit. Bedding often obscured by	Spruce, aspen, soapberry.			No WRA (Clay Cliffs) Undisturbed in sample location.
20MK-018 (Uppe	Granodiorite	107	colluvial apron.	Very poorly drained.	699	60.7150N/135.0591W	
				Spruce and pine forest.			WRA present in overlying sediment. Regular foot traffic on sand, dug into face for undisturbed sampling surface.
			Fluvial sand overlying glaciolacustrine deposit. Well-sorted sand with evident bedding, overlain by loess and	Soapberry, kinnikinnick, fireweed groundcover.			
20MK-018 (Sand	Granodiorite	112	organics.	Poorly drained.	704	60.7147N/135.0591W	
			0-5 cm: Organics and WRA 5-13 cm: Oxidized loess 13-65+ cm: Clast-supported gravel 35% coarse sand matrix, 65% clasts (50% cobbles, 50% pebbles)	Aspen forest due to clearing on property. Spruce and pine forest surrounding. Soapberry, fireweed, kinnikinnick, and rosehip groundcover.			
20MK-019	Granodiorite	18		Well-drained.	765	60.5976N/134.9628W	Continuous WRA, undulating contact with underlying loess.
			0-5 cm: Organics and WRA 5-12 cm: Oxidized loess 12+ cm: Clast-supported gravel Coarse sand matrix	Open, mature spruce forest. Soapberry, lupine, kinnikinnick, and grass groundcover.			Continuous WRA. Small roots to 47 cm.
20MK-020	Granodiorite	27.5	40% cobbles, 60% pebbles	Well drained.	754	60.6110N/134.9770W	
			0-3 cm: Organics	Submature to mature pine and spruce.			No WRA observed.

			3-22 cm: Loess 22-70 cm: Till Poorly sorted clasts in fine- to medium-grained sandy matrix with minor silt. 60% matrix, 40% clasts 40% small boulders, 20% cobbles,	Extensive kinnikinnick, with interspersed fireweed, soapberry, lupine. Poorly drained.			Grown-over tire ruts.
20MK-021	Granodiorite	>6.8	40% pebbles		785	60.6976N/135.1071W	
			0-4 cm: Organics 4-20 cm: Loess 21-60 cm: Fine-grained till Sub-angular to sub-rounded clasts in silty fine-grained sand matrix. 15% clasts, 85% matrix. 60% cobbles, 40% pebbles. Clast concentration increases with depth to 60% matrix,	Spruce and willow trees with some pine. Cranberry, soapberry, lupine, feather moss groundcover.			Discontinuous WRA. Roots to 40 cm.
20MK-022	Granodiorite	>3	40% clasts at 65 cm.	Moderately well-drained.	776	60.7043N/135.1011W	
			0-8 cm: Organics and WRA 8-30 cm: Loess 30-60+ cm: Gravel Sub-angular to sub-rounded clasts in a coarse-grained sand matrix. 60% matrix, 40% sand. 30% small boulders, 40% cobbles,	Spurce and pine forest with willow saplings. Soapberry groundcover with feather moss patches. Moderately well-drained.			
20MK-023	Mandanna sedimer	>30	30% pebbles.		745	60.7680N/135.1294W	Discontinuous lenses of WRA.
			0-3 cm: Organics 3-26 cm: Loess 26-60 cm: Gravel with medium- to coarse-grained sand matrix. 30% matrix, 70% clasts. 20% small boulders, 50% cobbles,	Open spruce forest with some aspen. Kinnikinnick, soapberry, and rosehip groundcover. Well drained.			
20MK-024	Mandanna sedimer	21	30% pebbles.		730	60.7787N/135.1468W	No WRA observed.
			0-3 cm: Organics 3-22 cm: Medium-grained sand with silt. 60% sand, 40% silt. 22-60 cm: Medium-grained sand, well-sorted with negligible silt.	Scraggly immature pine, pine needle and kinnikinnick groundcover. Well drained.			No WRA observed. Evidence of old ATV trail, surface disturbance only. Roots to 16cm, fine roots to 28 cm.
20MK-025	Unknown	>100			677	60.7752N/135.1065W	
			0-3 cm: Organics 3-35 cm: Extremely compacted white loess. Highly undulating contact with sand, some lobes and lenses extend 15 cm into underlying sand. 35-60+ cm: Medium- to fine-grained sand. Less compacted than overlying layer.	Scraggly, immature spruce and pine. Sparse groundcover, consisting where it exists of lichen, kinnikinnick, and patches of mossberry. Well drained.			Discontinuous WRA. Some evidence of old trails. Lots of stumps, may be an old woodlot.
20MK-026	Unknown	108			682	60.7808N/135.1154W	Fine roots to 55 cm.
			0-3 cm: Organics 3-10 cm: Loess 10-21cm: Medium to fine-grained, brick-red oxidized sand 21-60+ cm: Fine to very fine-grained	Submature spruce and pine with some aspen and willow. Ground mostly covered with pine needles, some soapberry and grass.			
20MK-027	Basalt	31	sand, no pebbles	Well-drained.	642	60.6976N/135.0260W	Discontinuous WRA.
			0-4 cm: Organics 4-25 cm: Gravel 85% clasts, 15% sandy matrix. 60% cobbles, 40% pebbles. 25-60 cm: Gravelly sand 75% sand matrix, 25% clasts. Sand is fine- to medium-grained, interspersed with sub-rounded pebble	Spruce forest with some pine, willow, and aspen. Feather moss groundcover to SE, grass groundcover to NW. Fireweed and soapberry throughout. Well drained.			No WRA observed. Fine roots to 35 cm.
20MK-028	Granodiorite	>93	and cobbles.		659	60.7020N/135.0129W	

Appendix 2 – Grain size data

Site	< 3 inches	< 19 mm	< 8 mm	< 4 mm	< 2 mm	< #10 (2 mm)	< #18 (1 mm)	< #35 (0.5 mm)
	%	%	%	%	%	%	%	%
20MK-001	10.6	6.9	9.6	4.6	68.3	6.4	8.9	10.6
20MK-002	50.3	14.2	10.7	9.2	15.6	27.4	35.2	17.6
20MK-003	7.8	25.4	30.4	17.6	18.8	33.6	27.9	21.1
20MK-004		8.3	8.5	6.7	76.5	4.9	7.8	10.8
20MK-005	8.9	11.7	7.2	7.1	65.1	5.1	7.6	13.8
20MK-006				0.4	99.6	0.3	2.4	6.8
20MK-007				0.4	99.6	0.3	0.7	1.0
20MK-008	4.7	26.6	17.9	9.8	41.0	6.8	21.1	32.2
20MK-009	33.9	28.3	7.5	5.0	25.3	9.1	28.7	33.6
20MK-010	3.2	26.3	18.6	20.7	31.2	31.3	26.1	17.3
20MK-013					100.0		2.1	52.4
20MK-014	39.3	20.9	9.5	4.8	25.5	20.1	28.3	17.3
20MK-014	21.0	35.2	12.1	6.6	25.1	21.3	29.6	21.2
20MK-015		11.7	6.1	5.3	76.9	3.8	6.1	10.2
20MK-016	6.0	41.0	18.0	8.0	27.0	9.7	14.0	24.9
20MK-017		0.9	0.1	0.2	98.8	0.6	0.4	1.1
20MK-019	35.7	21.9	14.7	10.4	17.3	28.0	29.3	20.6
20MK-020	11.2	33.1	7.9	4.4	43.4	7.5	37.6	41.7
20MK-021	11.9	18.3	10.1	6.7	53.0	5.4	11.7	15.3
20MK-022	12.3	10.0	5.5	4.9	67.3	6.1	9.1	13.4
20MK-023		24.1	14.0	16.8	45.1	24.4	36.8	17.2
20MK-024	11.7	26.2	15.2	14.7	32.2	28.6	30.1	18.0
20MK-025					100.0	0.1	2.2	48.9
20MK-026				0.1	99.9		0.8	80.2
20MK-027					100.0	0.1	0.6	7.4
20MK-028	15.2	11.8	5.0	4.3	63.7	4.1	13.8	37.5

< # 60 (0.25 mm)	< # 140 (0.105 mm)	< 53 micron	< 2 micron
%	%	%	%
18.2	6.7	33.5	15.7
7.8	1.5	7.6	2.9
7.9	1.5	6.1	1.9
16.1	6.1	33.0	21.3
26.7	8.3	32.2	6.3
8.8	6.8	70.8	4.1
4.0	6.0	80.6	7.4
17.7	4.1	14.3	3.8
15.0	2.4	8.3	2.9
10.4	2.6	9.1	3.2
33.3	10.2	1.9	0.1
8.9	2.4	15.5	7.5
9.8	2.1	11.0	5.0
22.8	9.6	37.1	10.4
31.8	6.0	9.7	3.9
57.4	18.3	15.5	6.7
8.6	2.2	8.9	2.4
6.7	1.3	3.4	1.8
29.2	9.1	25.4	3.9
26.7	10.3	31.0	3.4
8.4	2.4	7.9	2.9
8.2	2.6	10.0	2.5
46.6	0.8	0.9	0.5
16.6	0.6	0.9	0.9
37.7	19.4	31.9	2.9
30.6	4.8	6.1	3.1

Appendix 3A – Matrix geochemistry

Method	ME-XRF26	ME-XRF262	ME-XRF263	ME-XRF264	ME-XRF265	ME-XRF266	ME-XRF267
Element	Al2O3	BaO	CaO	Cr2O3	Fe2O3	K2O	MgO
	%	%	%	%	%	%	%
20MK-001A	11.65	0.12	11.20	<0.01	4.04	1.74	2.23
20MK-002A	14.98	0.11	4.14	0.02	7.75	1.78	4.33
20MK-003A	14.57	0.12	3.36	0.01	6.40	1.79	3.41
20MK-004A	14.38	0.12	3.05	0.01	4.99	2.02	2.21
20MK-005A	13.66	0.13	2.51	0.01	3.86	2.21	1.36
20MK-006A	13.06	0.14	2.80	0.01	3.59	2.31	1.70
20MK-007A	13.23	0.14	2.78	0.01	3.61	2.39	1.50
20MK-008A	14.74	0.13	3.13	0.01	5.50	2.17	2.30
20MK-009A	14.80	0.12	2.47	0.01	5.96	2.17	1.94
20MK-010A	15.45	0.10	4.52	0.02	7.05	1.65	3.95
20MK-013A	13.27	0.13	2.77	0.02	5.41	2.24	1.68
20MK-014A	14.15	0.13	2.53	0.01	5.19	2.12	1.72
20MK-014A (duplicate)	14.10	0.13	2.50	0.01	5.28	2.18	1.70
20MK-015A	13.99	0.13	2.34	0.01	3.94	2.26	1.34
20MK-016A	13.15	0.13	2.75	0.04	6.01	2.01	1.80
20MK-017A	13.19	0.14	2.26	0.02	3.82	2.28	1.72
20MK-018	12.60	0.14	6.26	0.01	4.65	2.04	2.49
20MK-019A	14.58	0.13	2.38	0.01	5.23	2.37	1.87
20MK-020A	14.29	0.12	2.71	0.01	6.21	2.37	1.86
20MK-021A	13.71	0.13	2.71	0.01	3.71	2.15	1.46
20MK-022A	13.53	0.12	2.81	0.01	3.76	2.19	1.37
20MK-023A	14.27	0.12	4.30	0.01	7.25	1.95	3.50
20MK-024A	14.22	0.12	4.17	0.02	6.40	2.07	3.56
20MK-025A	12.80	0.13	2.78	0.02	4.08	2.25	1.58
20MK-026A	14.03	0.13	3.53	0.05	6.75	2.09	2.62
20MK-027A	12.80	0.14	2.54	0.02	3.63	2.25	1.57
20MK-028A	12.60	0.13	2.51	0.02	4.38	2.23	1.74

ME-XRF268	ME-XRF269	ME-XRF2610	ME-XRF2611	ME-XRF2612	ME-XRF2613	OA-GRA05x	ME-XRF2614
MnO	Na2O	P2O5	SiO2	SrO	TiO2	LOI 1000	Total
%	%	%	%	%	%	%	%
0.07	2.62	0.22	53.23	0.06	0.55	11.57	99.43
0.10	2.45	0.23	55.87	0.06	0.70	7.48	100.15
0.10	2.71	0.23	56.85	0.06	0.75	9.39	99.90
0.08	3.11	0.17	64.23	0.05	0.64	3.90	99.05
0.05	3.43	0.12	69.75	0.06	0.51	1.96	99.70
0.06	3.26	0.20	70.11	0.05	0.50	1.75	99.62
0.06	3.22	0.18	68.96	0.04	0.52	2.67	99.39
0.09	3.17	0.21	64.02	0.06	0.65	3.32	99.68
0.07	2.84	0.14	61.36	0.05	0.60	6.36	98.99
0.11	2.83	0.20	55.55	0.05	0.89	6.83	99.35
0.08	3.15	0.16	68.64	0.05	0.67	1.56	99.95
0.17	2.74	0.15	61.41	0.04	0.60	8.72	99.81
0.08	2.88	0.13	63.07	0.05	0.61	6.56	99.41
0.05	3.41	0.12	69.69	0.05	0.54	1.97	99.91
0.07	3.02	0.12	67.33	0.05	0.75	2.56	99.92
0.06	3.06	0.14	70.82	0.05	0.49	1.99	100.15
0.08	2.61	0.23	62.51	0.04	0.60	4.68	99.03
0.09	3.05	0.16	64.46	0.05	0.58	4.29	99.36
0.08	3.16	0.23	65.69	0.05	0.65	2.64	100.20
0.05	3.58	0.13	69.68	0.06	0.57	1.43	99.46
0.05	3.60	0.17	70.15	0.06	0.56	1.15	99.62
0.10	2.74	0.37	59.56	0.06	0.80	4.13	99.30
0.09	2.91	0.25	60.45	0.06	0.70	4.54	99.71
0.07	3.22	0.13	70.85	0.05	0.56	1.25	99.88
0.10	3.06	0.24	63.26	0.05	1.03	2.19	99.29
0.06	3.24	0.14	70.66	0.05	0.51	1.42	99.14
0.06	3.07	0.16	70.30	0.04	0.55	1.56	99.45

C-IR07	S-IR08	ME-MS81	ME-MS8115	ME-MS8116	ME-MS8117	ME-MS8118	ME-MS8119
C	S	Ba	Ce	Cr	Cs	Dy	Er
%	%	ppm	ppm	ppm	ppm	ppm	ppm
3.48	0.01	1040	44.6	50	2.60	2.87	1.69
2.23	0.01	1015	70.1	130	3.31	3.53	1.94
3.36	0.02	1035	59.7	80	3.05	2.87	1.70
0.76	<0.01	1045	57.4	80	3.07	4.11	2.21
0.31	<0.01	1095	54.2	60	2.03	3.05	1.63
0.25	<0.01	1245	46.6	80	2.03	3.56	2.06
0.60	<0.01	1110	42.2	60	1.92	3.60	2.11
0.56	<0.01	1150	57.4	70	3.75	3.39	2.02
1.92	0.01	1060	49.9	80	4.64	2.73	1.49
1.88	<0.01	974	67.9	140	5.73	4.35	2.33
0.10	<0.01	1200	102.0	170	1.61	4.39	2.41
3.36	0.01	1215	62.1	80	3.99	3.12	1.63
2.31	0.02	1115	67.3	90	3.64	3.82	2.10
0.22	<0.01	1205	42.1	60	2.07	2.91	1.57
0.60	0.01	1240	60.2	240	2.36	3.81	2.00
0.14	<0.01	1290	38.8	70	2.01	2.94	1.69
0.91	0.01	1315	44.1	100	2.44	3.49	2.04
1.16	<0.01	1135	71.8	70	4.39	3.66	1.87
0.43	<0.01	1095	65.0	70	3.47	3.70	1.99
0.13	0.01	1085	53.7	60	1.69	2.53	1.45
0.10	0.01	1125	48.3	60	1.60	2.94	1.84
0.66	0.01	1095	88.1	90	2.88	5.42	2.95
1.15	0.02	1070	57.8	140	3.32	4.95	2.82
0.08	0.01	1290	94.6	140	1.85	4.28	2.44
0.20	0.01	1200	150.5	360	2.51	6.38	3.50
0.10	0.01	1365	49.7	140	1.97	3.14	1.96
0.16	0.01	1260	48.3	180	1.85	3.41	1.95

ME-MS8120	ME-MS8121	ME-MS8122	ME-MS8123	ME-MS8124	ME-MS8125	ME-MS8126	ME-MS8127
Eu	Ga	Gd	Ge	Hf	Ho	La	Lu
ppm	ppm	ppm	ppm	ppm	ppm	ppm	ppm
0.91	14.0	3.14	<5	4.5	0.53	23.5	0.26
1.13	18.0	4.01	<5	3.8	0.69	27.2	0.27
1.00	18.0	3.64	<5	4.8	0.59	27.6	0.24
1.17	16.7	4.54	<5	4.9	0.73	32.0	0.32
1.01	14.7	3.38	<5	5.8	0.57	30.3	0.25
0.90	14.8	3.75	<5	5.1	0.72	24.3	0.31
0.91	14.0	3.90	<5	6.5	0.66	24.1	0.35
0.99	17.3	3.68	<5	5.8	0.63	30.1	0.31
0.78	17.0	2.85	<5	5.5	0.50	26.0	0.24
1.38	17.9	4.84	<5	4.2	0.79	29.6	0.31
1.21	15.5	5.68	<5	13.4	0.86	57.3	0.44
0.95	17.3	3.55	<5	5.2	0.61	33.9	0.27
1.15	15.8	4.02	<5	7.4	0.73	34.8	0.35
0.89	16.1	3.42	<5	5.2	0.50	24.1	0.27
1.17	16.5	4.17	<5	8.2	0.76	34.6	0.33
0.92	14.9	3.37	<5	3.0	0.53	23.6	0.23
1.06	14.3	3.99	<5	3.8	0.73	23.8	0.28
1.00	16.5	4.12	<5	5.2	0.66	32.1	0.31
1.04	16.7	4.35	<5	6.5	0.71	30.2	0.35
0.86	14.6	2.79	<5	5.9	0.54	26.2	0.23
0.99	15.0	3.32	<5	5.8	0.60	26.1	0.28
1.72	18.7	6.42	<5	11.2	1.11	53.4	0.50
1.47	16.9	5.86	<5	8.8	1.00	35.1	0.44
1.20	15.9	4.71	<5	8.7	0.78	54.7	0.33
1.60	18.1	7.70	<5	12.3	1.22	84.8	0.53
0.97	15.1	3.71	<5	6.7	0.66	28.6	0.32
1.00	14.8	3.72	<5	7.4	0.67	24.3	0.27

ME-MS8128	ME-MS8129	ME-MS8130	ME-MS8131	ME-MS8132	ME-MS8133	ME-MS8134	ME-MS8135
Nb	Nd	Pr	Rb	Sm	Sn	Sr	Ta
ppm	ppm	ppm	ppm	ppm	ppm	ppm	ppm
8.0	18.4	5.04	51.1	3.77	1	581	0.7
8.3	23.8	6.25	56.6	5.16	1	510	0.6
9.0	22.3	5.91	60.5	4.52	1	473	0.6
9.4	26.4	7.04	60.0	5.46	1	460	0.7
8.6	21.5	6.09	64.2	4.22	1	487	0.7
9.7	20.4	5.41	65.7	4.57	2	411	0.8
10.2	20.2	5.30	64.9	4.28	2	332	1.0
9.0	23.7	6.25	59.7	4.90	2	447	0.7
9.7	20.9	5.53	65.2	4.00	1	377	0.9
11.9	27.3	6.92	64.9	6.12	2	470	0.9
14.9	41.1	11.70	61.8	7.24	2	379	1.6
8.7	25.2	6.87	72.6	5.06	1	368	0.7
10.4	27.2	7.27	77.3	5.11	1	366	0.7
8.0	19.2	5.22	62.5	4.19	1	450	0.6
10.9	27.5	7.09	61.9	5.40	1	411	1.0
7.5	20.0	5.09	65.2	4.17	2	370	0.6
9.7	20.4	5.21	58.8	4.14	2	382	0.7
9.0	25.7	6.98	73.0	5.35	1	374	0.7
9.7	26.4	7.05	70.1	5.51	1	402	0.8
9.0	19.3	5.39	57.1	3.39	1	481	0.6
9.8	22.3	6.00	60.1	4.48	1	498	0.7
10.8	41.1	10.90	59.2	7.43	1	494	0.7
8.5	31.4	7.85	66.5	6.71	1	499	0.8
17.5	37.5	10.40	72.1	6.46	2	449	1.8
19.1	58.5	16.80	63.2	9.79	2	438	2.2
8.8	21.2	5.85	69.1	3.85	1	451	1.1
11.0	20.2	5.39	67.2	4.04	1	420	1.1

ME-MS8136	ME-MS8137	ME-MS8138	ME-MS8139	ME-MS8140	ME-MS8141	ME-MS8142	ME-MS8143
Tb	Th	Tm	U	V	W	Y	Yb
ppm	ppm	ppm	ppm	ppm	ppm	ppm	ppm
0.46	8.81	0.21	2.40	91	2	15.7	1.54
0.59	11.55	0.26	2.86	161	2	17.2	1.59
0.50	15.65	0.24	3.29	129	3	15.5	1.48
0.70	10.35	0.31	2.47	105	2	22.8	2.00
0.55	9.28	0.23	2.46	110	2	15.2	1.57
0.60	7.72	0.29	2.23	81	2	19.7	2.01
0.58	7.98	0.31	3.10	72	2	18.4	2.14
0.57	9.36	0.27	3.05	113	2	17.1	1.96
0.44	7.62	0.24	2.25	103	2	14.3	1.66
0.70	12.10	0.36	3.41	156	2	21.2	2.23
0.79	11.95	0.41	3.36	112	2	23.4	2.84
0.50	10.75	0.27	2.36	99	2	15.8	1.79
0.63	10.75	0.32	2.96	103	2	19.3	1.90
0.44	7.11	0.24	2.24	98	2	14.8	1.79
0.62	8.36	0.32	3.37	128	3	20.1	2.19
0.47	7.59	0.22	3.04	84	2	15.2	1.65
0.60	6.50	0.30	2.28	126	3	20.0	1.78
0.63	10.40	0.31	2.67	104	2	17.5	1.98
0.60	9.49	0.29	2.83	114	2	18.5	1.98
0.43	8.55	0.22	2.30	84	4	13.5	1.55
0.53	7.56	0.24	2.52	88	2	15.3	1.64
0.87	13.35	0.47	3.81	155	3	31.2	3.29
0.85	9.83	0.39	2.50	140	2	28.0	2.61
0.73	13.55	0.30	2.92	106	2	22.8	2.30
1.08	20.90	0.50	4.06	163	2	34.8	3.58
0.53	7.29	0.27	2.05	95	2	18.0	1.81
0.56	7.25	0.24	2.70	99	2	18.1	1.77

ME-MS8144	ME-MS42	ME-MS4245	ME-MS4246	ME-MS4247	ME-MS4248	ME-MS4249	ME-MS4250
Zr	As	Bi	Hg	In	Re	Sb	Sc
ppm	ppm	ppm	ppm	ppm	ppm	ppm	ppm
179	12.1	0.16	0.014	0.016	<0.001	0.71	3.5
143	26.9	0.40	0.012	0.029	<0.001	0.85	6.1
191	18.6	0.53	0.013	0.028	<0.001	0.62	4.9
196	14.1	0.21	0.014	0.020	<0.001	0.69	5.0
235	9.4	0.14	0.009	0.014	<0.001	0.39	3.7
204	7.9	0.12	0.019	0.012	0.001	0.50	3.0
228	7.6	0.13	0.022	0.016	0.001	0.30	2.9
216	20.7	0.34	0.008	0.019	<0.001	2.48	4.2
222	31.8	0.30	0.013	0.024	<0.001	0.77	3.7
164	19.8	0.24	0.021	0.027	<0.001	0.57	5.4
524	6.7	0.18	0.017	0.014	<0.001	0.45	3.8
196	16.6	0.20	0.016	0.022	<0.001	0.69	4.6
302	16.2	0.22	0.024	0.020	<0.001	0.59	4.4
218	10.5	0.10	0.005	0.015	<0.001	0.41	4.1
351	10.8	0.10	0.014	0.014	<0.001	0.51	4.3
123	11.5	0.22	<0.005	0.014	<0.001	0.49	3.7
151	7.9	0.13	0.033	0.019	<0.001	0.66	5.1
194	26.4	0.22	0.01	0.024	<0.001	0.74	4.8
274	18.9	0.20	0.009	0.020	<0.001	0.63	4.0
233	8.2	0.10	0.006	0.010	<0.001	0.32	2.3
233	7.3	0.08	0.007	0.009	<0.001	0.30	2.4
484	16.2	0.50	0.014	0.026	<0.001	0.80	7.4
343	18.0	0.30	0.018	0.020	<0.001	0.87	6.7
327	5.5	0.07	0.007	0.010	<0.001	0.39	2.4
483	7.2	0.16	0.011	0.021	<0.001	0.52	5.3
238	7.9	0.08	0.025	0.012	<0.001	0.44	2.7
285	22.9	0.07	0.007	0.010	<0.001	0.30	2.3

ME-MS4251	ME-MS4252	ME-MS4253	ME-4ACD81	ME-4ACD8154	ME-4ACD8155	ME-4ACD8156
Se	Te	Tl	Ag	Cd	Co	Cu
ppm	ppm	ppm	ppm	ppm	ppm	ppm
0.3	0.04	0.11	<0.5	<0.5	10	55
0.5	0.07	0.16	<0.5	<0.5	23	64
0.2	0.04	0.15	<0.5	<0.5	20	80
0.2	0.03	0.13	<0.5	<0.5	12	41
0.3	0.02	0.09	<0.5	<0.5	8	24
<0.2	0.02	0.06	<0.5	<0.5	9	30
0.2	0.02	0.07	<0.5	<0.5	7	94
0.7	0.05	0.13	<0.5	<0.5	11	522
0.4	0.08	0.13	<0.5	<0.5	17	39
0.4	0.06	0.17	<0.5	<0.5	20	54
0.3	0.02	0.06	<0.5	<0.5	12	15
0.3	0.04	0.15	<0.5	<0.5	15	33
0.3	0.05	0.15	0.5	<0.5	14	28
0.3	0.02	0.11	<0.5	<0.5	7	22
<0.2	0.02	0.09	<0.5	<0.5	11	26
0.2	0.01	0.06	<0.5	<0.5	9	22
0.2	0.02	0.09	<0.5	<0.5	13	33
0.4	0.05	0.19	<0.5	<0.5	14	35
0.3	0.04	0.19	<0.5	<0.5	11	27
<0.2	0.02	0.07	<0.5	<0.5	9	19
<0.2	0.02	0.06	<0.5	<0.5	8	18
0.3	0.05	0.15	<0.5	0.5	16	179
0.3	0.04	0.20	0.5	<0.5	16	61
<0.2	0.01	0.05	<0.5	<0.5	8	15
<0.2	0.03	0.13	<0.5	<0.5	15	26
<0.2	0.02	0.05	<0.5	<0.5	8	22
<0.2	0.01	0.05	<0.5	<0.5	8	13

ME-4ACD8157	ME-4ACD8158	ME-4ACD8159	ME-4ACD8160	ME-4ACD8161	ME-4ACD8162
Li	Mo	Ni	Pb	Sc	Zn
ppm	ppm	ppm	ppm	ppm	ppm
20	1	27	12	9	56
20	2	61	21	18	80
30	3	57	16	14	84
20	<1	36	10	12	63
10	<1	19	13	10	36
20	<1	28	13	10	50
20	3	26	14	10	50
20	9	32	19	12	72
20	2	34	23	11	72
30	1	72	21	15	101
10	1	37	15	13	62
20	<1	33	17	12	89
20	2	33	20	11	71
10	<1	23	10	10	41
20	1	41	12	12	51
20	<1	37	9	11	51
20	1	46	9	13	71
20	1	32	23	13	78
20	1	28	20	12	68
10	1	22	13	9	40
10	1	21	15	10	38
30	12	42	19	16	84
20	3	48	21	15	72
10	<1	28	15	10	43
20	1	58	14	16	87
10	1	36	12	10	41
10	<1	29	11	10	45

Appendix 3B – Clast geochemistry

Method	ME-XRF26	ME-XRF262	ME-XRF263	ME-XRF264	ME-XRF265	ME-XRF266
Element	Al2O3	BaO	CaO	Cr2O3	Fe2O3	K2O
	%	%	%	%	%	%
Granite 20MK-005	15.42	0.10	3.34	<0.01	4.44	2.50
Granite 20MK-010	17.68	0.17	4.68	<0.01	6.36	2.73
Granite 20MK-023	16.54	0.15	5.19	0.01	5.23	1.97
Granite 20MK-020	17.39	0.19	6.49	0.01	7.51	2.67
Limestone 20MK-010	0.95	0.01	53.20	<0.01	0.45	0.04
Limestone 20MK-024	0.92	0.01	46.10	<0.01	0.67	0.05
Basalt 20MK-010	14.75	0.06	9.64	0.04	12.49	1.26
Basalt 20MK-016	14.85	0.06	8.85	0.05	12.70	0.74
Volcani 20MK-005	17.19	0.22	4.80	0.02	7.04	2.17
Volcanic 20MK-009	14.52	0.17	0.87	<0.01	2.99	4.74
Volcanic 20MK-017	16.45	0.11	6.67	0.03	8.28	1.52
Volcanic 20MK-015	15.94	0.15	8.01	0.03	10.39	0.93
Volcaniclastic 20MK-004/-021	15.56	0.17	5.33	0.01	5.78	2.74
Volcaniclastic 20MK-016	14.68	0.03	9.70	0.03	10.84	0.20
Clastic sedimentary 20MK-024	16.59	0.19	2.48	<0.01	5.80	3.61
Clastic sedimentary 20MK-001/-002/-003	15.54	0.15	3.22	0.01	5.85	2.35
Clastic sedimenary 20MK-009	16.41	0.16	2.80	0.01	6.36	3.50
Clastic sedimentary 20MK-017	15.72	0.22	4.12	0.01	5.00	2.22
Phenocrystic 20MK-005	15.15	0.15	3.56	0.02	4.71	3.47
Phenocrystic 20MK-010	16.26	0.24	4.49	0.01	7.28	2.97
Phenocrystic 20MK-015	15.24	0.16	1.84	<0.01	3.57	3.23
Phenocrystic 20MK-024	16.82	0.13	3.91	<0.01	5.87	1.44

ME-XRF267	ME-XRF268	ME-XRF269	ME-XRF2610	ME-XRF2611	ME-XRF2612	ME-XRF2613	OA-GRA05x
MgO	MnO	Na2O	P2O5	SiO2	SrO	TiO2	LOI 1000
%	%	%	%	%	%	%	%
2.10	0.07	4.23	0.17	66.59	0.07	0.44	0.70
2.26	0.13	4.93	0.36	58.29	0.07	1.10	0.62
3.21	0.08	4.88	0.20	60.94	0.10	0.60	0.76
4.02	0.13	3.51	0.24	55.12	0.09	0.97	1.18
0.71	0.03	<0.01	0.04	3.84	0.05	0.03	40.42
6.66	0.02	<0.01	0.04	6.33	0.14	0.03	38.84
7.30	0.17	3.24	0.61	47.80	0.09	1.78	0.63
7.19	0.17	3.11	0.38	47.66	0.07	1.98	1.05
4.07	0.12	4.26	0.34	55.56	0.11	0.81	2.58
0.50	0.05	3.65	0.07	70.89	0.04	0.25	0.59
5.20	0.14	3.39	0.28	54.93	0.08	0.87	1.41
5.72	0.20	3.64	0.25	50.72	0.07	1.40	1.77
2.20	0.07	2.65	0.24	61.82	0.08	0.59	2.60
6.16	0.17	3.31	0.16	51.28	0.02	1.58	1.95
2.12	0.10	3.67	0.28	61.27	0.08	0.58	2.65
2.95	0.08	3.06	0.26	63.00	0.08	0.56	2.38
2.50	0.08	3.29	0.30	61.40	0.07	0.61	2.17
2.48	0.08	3.37	0.24	64.22	0.11	0.49	1.53
2.85	0.09	3.71	0.16	64.19	0.05	0.49	0.96
3.59	0.11	3.51	0.40	58.25	0.11	0.94	1.99
0.66	0.08	4.60	0.10	69.85	0.05	0.28	0.57
2.20	0.09	5.18	0.22	61.81	0.10	0.63	1.80

ME-XRF2614	C-IR07	S-IR08	ME-MS81	ME-MS8115	ME-MS8116	ME-MS8117	ME-MS8118	ME-MS8119
Total	C	S	Ba	Ce	Cr	Cs	Dy	Er
%	%	%	ppm	ppm	ppm	ppm	ppm	ppm
100.25	0.03	<0.01	928	57.0	30	1.00	1.93	1.12
99.52	0.02	<0.01	1595	81.0	20	1.97	5.75	3.42
99.98	0.03	<0.01	1420	57.7	70	0.71	2.97	1.64
99.70	0.01	0.01	1740	50.1	50	2.65	4.02	2.36
99.85	11.10	<0.01	62	5.5	10	0.06	0.49	0.31
99.86	9.98	<0.01	34.8	2.5	10	0.12	0.34	0.17
100.05	0.14	<0.01	535	61.7	300	0.21	4.17	1.74
99.05	0.04	<0.01	457	39.2	330	0.06	4.95	2.13
99.46	0.19	0.01	2130	45.8	150	3.43	4.22	2.08
99.41	0.03	<0.01	1535	55.9	10	3.18	3.36	1.98
99.68	0.03	0.05	974	42.7	200	2.88	3.33	1.96
99.43	0.01	<0.01	1375	37.6	160	0.52	4.96	3.00
107.90	0.02	3.35	1485	43.4	70	0.78	3.37	2.12
100.55	0.09	0.09	229	14.0	230	0.48	6.11	3.39
99.60	0.38	0.02	1650	49.6	40	2.85	3.42	1.71
99.73	0.20	0.04	1325	29.6	80	2.37	2.69	1.56
101.15	0.29	0.5	1525	36.0	90	17.75	2.51	1.56
100.15	0.11	0.1	2060	38.4	50	1.60	2.83	1.77
99.67	0.06	<0.01	1320	61.9	110	2.26	3.85	2.30
100.30	0.08	0.01	2170	84.5	90	3.72	4.57	2.27
100.30	0.02	<0.01	1425	56.7	30	1.47	3.40	2.62
100.30	0.22	<0.01	1115	39.8	30	0.58	2.52	1.48

ME-MS8120	ME-MS8121	ME-MS8122	ME-MS8123	ME-MS8124	ME-MS8125	ME-MS8126	ME-MS8127
Eu	Ga	Gd	Ge	Hf	Ho	La	Lu
ppm	ppm	ppm	ppm	ppm	ppm	ppm	ppm
0.88	20.30	2.86	<5	4.4	0.39	34.9	0.18
1.73	21.90	6.50	<5	6.1	1.16	42.9	0.48
1.16	21.40	3.59	<5	4.5	0.54	31.2	0.25
1.34	20.50	4.40	<5	4.9	0.84	27.6	0.36
0.13	1.20	0.53	<5	0.2	0.10	3.7	0.06
0.14	1.30	0.42	<5	0.2	0.07	2.4	0.03
1.92	21.90	5.46	<5	3.8	0.78	32.3	0.22
1.85	24.30	5.87	<5	3.6	0.83	23.3	0.24
1.37	20.50	4.61	<5	3.6	0.86	25	0.31
0.66	19.10	3.20	<5	6.2	0.76	28.5	0.32
1.29	22.30	4.26	<5	3.8	0.68	22.2	0.26
1.50	21.20	5.12	<5	3.2	1.06	18.1	0.40
0.91	19.80	4.04	<5	2.9	0.69	24.2	0.32
1.42	17.60	5.54	<5	3.2	1.35	5.3	0.54
1.09	20.10	4.03	<5	3.9	0.69	28.1	0.31
0.90	17.60	3.23	<5	2.3	0.58	15.8	0.22
0.89	21.80	3.20	<5	2.9	0.61	19.5	0.23
0.97	19.00	3.08	<5	3.6	0.61	19.5	0.25
1.02	19.80	4.28	<5	4.4	0.79	32.2	0.33
1.77	19.90	5.71	<5	4.5	0.80	42.9	0.36
0.80	21.30	3.59	<5	5.6	0.78	30.3	0.41
1.00	19.60	2.94	<5	3.2	0.53	21.6	0.20

ME-MS8128	ME-MS8129	ME-MS8130	ME-MS8131	ME-MS8132	ME-MS8133	ME-MS8134	ME-MS8135
Nb	Nd	Pr	Rb	Sm	Sn	Sr	Ta
ppm	ppm	ppm	ppm	ppm	ppm	ppm	ppm
5.1	19.7	5.96	67.1	3.33	1	597.0	0.4
13.7	36.8	9.87	70.4	7.33	2	619.0	1.0
6.7	24.2	6.75	44.8	4.79	1	901.0	0.5
9.0	22.3	5.86	70.9	4.67	1	801.0	0.7
0.5	2.3	0.69	1.5	0.52	<1	437.0	0.1
0.3	2.0	0.41	1.6	0.45	<1	1275.0	0.1
40.9	29.4	7.60	13.0	6.28	1	838.0	2.6
21.2	23.8	5.89	4.4	5.63	1	600.0	1.4
9.1	23.2	5.87	47.8	4.74	1	1085.0	0.6
11.6	20.1	5.87	145.5	3.97	1	329.0	1.0
8.0	21.5	5.38	57.9	4.77	1	751.0	0.6
6.5	21.4	5.13	16.8	5.30	1	601.0	0.5
9.3	20.3	5.40	66.2	4.40	1	667.0	0.7
3.5	12.7	2.44	2.5	4.20	1	176.5	0.3
8.8	24.8	6.38	98.3	4.60	1	693.0	0.7
5.8	15.5	3.92	53.0	3.24	1	634.0	0.4
6.5	17.6	4.57	115.0	3.55	1	614.0	0.6
7.0	18.8	4.61	58.5	3.77	2	979.0	0.4
8.8	26.0	6.90	106.0	5.61	2	404.0	0.5
9.0	39.1	10.10	73.6	7.41	2	861.0	0.5
11.2	23.2	6.15	83.5	4.04	2	344.0	0.8
4.8	18.5	4.70	27.2	4.06	1	863.0	0.2

ME-MS8136	ME-MS8137	ME-MS8138	ME-MS8139	ME-MS8140	ME-MS8141	ME-MS8142	ME-MS8143
Tb	Th	Tm	U	V	W	Y	Yb
ppm	ppm	ppm	ppm	ppm	ppm	ppm	ppm
0.34	16.15	0.16	4.72	86	1	10.2	1.14
0.98	11.90	0.50	3.09	135	1	32.5	3.36
0.54	14.35	0.26	3.65	122	1	16.1	1.57
0.70	7.91	0.32	2.08	184	1	22.6	2.19
0.07	0.32	0.05	3.63	23	1	4.3	0.34
0.06	0.20	0.03	0.69	19	2	2.5	0.24
0.79	3.61	0.27	0.56	167	1	20.0	1.63
0.84	2.00	0.29	0.75	204	<1	23.1	1.71
0.66	4.15	0.34	1.66	138	1	22.0	2.10
0.56	18.75	0.32	5.04	43	1	20.3	2.33
0.56	5.87	0.22	2.13	169	1	17.7	1.50
0.84	3.60	0.36	0.95	318	1	25.8	2.74
0.57	7.55	0.33	3.63	220	1	21.9	2.08
0.98	0.34	0.55	0.15	347	1	33.5	3.44
0.56	7.54	0.30	2.88	110	2	19.2	1.91
0.48	3.94	0.24	1.76	160	1	15.1	1.64
0.44	5.42	0.22	2.20	207	2	14.8	1.39
0.49	5.22	0.26	2.47	112	2	16.6	1.83
0.66	9.84	0.39	3.82	98	1	21.2	2.30
0.82	11.80	0.34	3.85	168	2	22.7	2.18
0.58	13.65	0.43	4.72	28	2	21.9	2.50
0.43	5.68	0.23	2.27	148	1	13.9	1.45

ME-MS8144	ME-MS42	ME-MS4245	ME-MS4246	ME-MS4247	ME-MS4248	ME-MS4249	ME-MS4250
Zr	As	Bi	Hg	In	Re	Sb	Sc
ppm	ppm	ppm	ppm	ppm	ppm	ppm	ppm
147	2.5	0.05	<0.005	0.005	<0.001	0.20	1.5
265	2.3	0.05	<0.005	0.013	<0.001	0.39	1.8
163	1.9	0.11	<0.005	0.010	<0.001	0.22	2.3
203	3.1	0.04	<0.005	0.009	<0.001	0.29	2.5
7	2.1	0.02	<0.005	<0.005	<0.001	0.10	0.7
7	3.9	<0.01	<0.005	0.016	<0.001	0.44	1.2
156	1.4	0.01	<0.005	0.018	<0.001	0.05	3.7
145	2.8	0.01	<0.005	0.018	<0.001	0.10	3.2
143	3.7	0.08	<0.005	0.023	0.001	0.62	5.0
230	9.6	0.11	<0.005	0.013	<0.001	0.50	2.8
149	8.3	0.18	<0.005	0.014	<0.001	1.03	3.6
119	5.2	0.04	<0.005	0.012	<0.001	0.23	3.6
99	18.7	1.41	<0.005	0.018	0.015	1.10	3.0
116	1.3	0.02	0.011	0.041	0.001	0.23	13.3
141	8.2	0.19	0.007	0.033	0.002	0.57	6.3
88	10.3	0.06	<0.005	0.027	<0.001	0.36	8.9
118	44	0.13	0.005	0.029	0.001	0.95	13.3
144	5.5	0.08	0.007	0.033	<0.001	0.32	4.8
159	2.1	0.02	<0.005	0.014	<0.001	0.36	3.7
175	3.7	0.07	<0.005	0.023	<0.001	0.32	6.1
225	0.8	0.19	<0.005	0.017	<0.001	0.09	1.5
127	1.7	0.03	<0.005	0.014	<0.001	0.23	3.9

ME-MS4251	ME-MS4252	ME-MS4253	ME-4ACD81	ME-4ACD8154	ME-4ACD8155	ME-4ACD8156	ME-4ACD8157
Se	Te	Tl	Ag	Cd	Co	Cu	Li
ppm	ppm	ppm	ppm	ppm	ppm	ppm	ppm
<0.2	<0.01	0.03	<0.5	<0.5	10	35	10
<0.2	<0.01	0.11	<0.5	<0.5	10	9	10
<0.2	<0.01	0.06	<0.5	<0.5	14	55	10
0.2	<0.01	0.07	<0.5	<0.5	19	16	20
0.5	0.01	<0.02	<0.5	0.6	1	15	<10
0.4	0.01	0.03	<0.5	<0.5	<1	10	<10
<0.2	<0.01	<0.02	<0.5	0.7	48	73	10
0.2	<0.01	0.03	<0.5	0.8	48	59	10
0.2	0.01	0.11	<0.5	0.5	19	14	30
0.2	0.01	0.1	<0.5	<0.5	3	8	10
0.2	0.01	0.21	<0.5	0.5	18	28	30
0.2	0.01	0.04	<0.5	0.6	32	42	10
7.2	1.18	0.05	<0.5	<0.5	12	14	10
0.3	0.01	0.03	<0.5	0.5	35	33	10
0.3	0.03	0.13	<0.5	<0.5	9	38	20
0.3	0.02	0.04	<0.5	<0.5	13	34	20
0.5	0.02	0.64	<0.5	<0.5	12	29	30
<0.2	0.01	0.05	<0.5	0.7	11	20	10
<0.2	0.01	0.06	<0.5	<0.5	12	8	20
<0.2	<0.01	0.13	<0.5	0.5	18	22	30
<0.2	0.01	0.03	<0.5	<0.5	3	3	20
0.2	0.01	0.02	<0.5	<0.5	11	18	10

ME-4ACD8158	ME-4ACD8159	ME-4ACD8160	ME-4ACD8161	ME-4ACD8162
Mo	Ni	Pb	Sc	Zn
ppm	ppm	ppm	ppm	ppm
2	12	21	7	45
1	6	11	14	73
1	27	7	12	51
<1	21	15	17	77
1	7	3	1	32
1	5	<2	1	23
1	190	2	22	105
1	195	2	19	114
<1	58	10	14	80
2	2	29	5	39
<1	54	10	15	78
1	55	8	28	89
15	59	16	14	31
<1	73	6	38	86
1	13	14	11	77
1	20	17	16	68
1	14	11	17	85
<1	9	13	13	96
1	36	9	11	69
<1	33	17	14	92
1	1	47	3	80
1	10	7	11	80